Thesis for the Master's degree in Molecular Biosciences
Main field of study in Molecular Biology

The importance of Gcn2 and Rad3 in cell-cycle regulation of the G2/M transition

Christiane Rothe

60 study points

Department of Molecular Biosciences
Faculty of mathematics and natural sciences
UNIVERSITY OF OSLO 06/2011

Abstract

Previously the existence of a Gcn2-dependent G1/S checkpoint which delays entry into S phase in response to ultraviolet (UVC) radiation had been shown. Moreover Gcn2 is active in S phase and G2 phase after UVC irradiation (Krohn *et al.*, 2008). Therefore we investigated whether Gcn2 also affects cell-cycle progression from G2 into mitosis. The classic checkpoint pathway is known to arrest cell-cycle progression in response to DNA damage in G2. The kinase Rad3 plays a central role in this checkpoint since mutants with a deletion of *rad3*Δ are checkpoint deficient after treatment with ionizing radiation. We therefore reasoned that if Gcn2 has a minor effect on cell-cycle progression after UVC irradiation, this could best be seen in a *rad3*Δ checkpoint mutant.

To explore this hypothesis, a *rad3*Δ*gcn2*Δ double mutant was made to study cell-cycle progression of synchronous cells after UVC irradiation in G2. Cell-cycle progression was monitored using a new flow cytometric method that conveniently measures the frequency of binuclear cells. The kinetics of entry into mitosis after UVC irradiation of *rad3*Δ and *rad3*Δ*gcn2*Δ cells were the same. We conclude that Gcn2 does not play a significant role in regulation of G2/M after UVC irradiation. Interestingly, while investigating the role of Gcn2 in the G2/M transition, we found that UVC-treated *rad3*Δ cells delay mitosis in the same way as wild type cells do. Despite lacking the *rad3* gene they elicit a checkpoint response to prevent entry into mitosis. This might indicate that other damage pathways exist. However, further studies are needed to characterize the checkpoint response in the absence of Rad3 and to uncover possible other players in the response to UV irradiation.

Contents

Chapter 1.

General introduction

Dysfunction of cell cycle checkpoints and DNA repair enzymes is known to be a characteristic of cancer cells (Krauss, 2008). Growth and proliferation of normal cells is carefully regulated by extracellular and intracellular signals. If those signal pathways are impaired, cells might escape the normal constraints on cell growth (increase in cell mass) and proliferation (increase in cell number) and thus cancer might develop. As cell division and replication are essential processes in cell proliferation, accumulation of changes in genes related to the cell-cycle or DNA repair is a major cause of cancer. Therefore the study of cell-cycle regulatory mechanisms and checkpoints are particularly relevant both to understand the processes leading to cancer development and as potential therapeutic targets.

Our group studies the G1/S transition using fission yeast (*Schizosaccharomyces pombe*) as a model organism. Tvegard *et al.* (2007) have identified a novel Gcn2-dependent checkpoint that regulates entry into S phase after treatment with ultraviolet (UVC) light. Furthermore, upon UVC irradiation the translation initiation factor eIF2α, a known target of Gcn2, becomes phosphorylated in G1, S and G2 phase (Krohn *et al.*, 2008). Phosphorylation of eIF2α mediated by Gcn2 is known as a stress response to amino acid deficiency leading to downregulation of global protein synthesis (Hinnebusch, 2005) but had not been linked to an UVC induced cell-cycle arrest before. Since at the G1/S transition Gcn2 is essential both for the translational downregulation and for the cell-cycle delay and in G2 Gcn2 is activated and downregulates translation (Krohn *et al.*, 2008), the question arises whether Gcn2 might also regulate the cell cycle at the G2/M transition. This is the subject of this master thesis.

Chapter 2.

Theoretical background

2.1. *Schizosaccharomyces pombe* as a model organism

Model organisms are simple organisms that allow to study and manipulate genes in order to understand fundamental mechanisms of cellular function. The choice of model organism often depends on the question being asked. Within animals, fungi, bacteria and plants various species are used as model organisms. Among fungi, *Schizosaccharomyces pombe*, is a very popular model used to study basic cellular mechanisms and their regulation. Failure of the corresponding pathways in human cells might lead to diseases. Therefore understanding the basic mechanisms in yeast is highly relevant for understanding the human diseases.

The fission yeast *S.pombe* is 3-4 µm in diameter and 7-15 µm in length. It has a typical eukaryotic cell cycle with G1, S, G2 and M phase and divides by binary fission (Moreno *et al.*, 1991). Cells are rod-shaped and have a simple structure where morphological changes can easily be observed. Sequencing of the genome by Wood *et al.* (2002) revealed that it has a size of 13,8 Mb coding for ~5000 genes distributed on three chromosomes. As fission yeast is not very specialized in evolutionary terms it is thought to represent genuine eukaryotic features which makes it an excellent model organism to study human disease genes; especially those involved in DNA damage and repair, cell-cycle control and recombination.

2.2. DNA damage

All living cells have to deal with DNA damage either caused by sun light and other naturally occurring DNA damaging agents or replication errors. Replication errors arise spontaneously when incorrect nucleotides are incorporated during replication. Normally the replication machinery removes these misincorporations

through its proofreading mechanism, but some errors might remain undetected. Mutagenic agents are another source of DNA damage. They include both chemicals and radiation (Brown, 2006). Base analogs, intercalating agents and alkylating agents belong to the group of chemical mutagens. Ultraviolet (UVC) and ionizing radiation (IR) are types of physical mutagens. UVC light induces covalent bonds between adjacent pyrimidines. The resulting dimers pose obstacles to the replicative DNA polymerase. IR is the most hazardous kind of radiation causing double strand breaks by attacking the DNA backbone (Watson *et al.*, 2008).

Both spontaneous mutations (e.g. replication errors) and mutations caused by mutagens have to be repaired to prevent loss of genetic information. Therefore DNA damage activates a checkpoint which inhibits cell-cycle progression, which in turn allows time for DNA repair. Alternatively, if the damage is too severe to be repaired, programmed cell death is triggered to eliminate the cells with unrepairable damage.

2.3. The cell cycle in fission yeast

The cell cycle is a series of events allowing cell duplication and division. Its goal is to produce two identical daughter cells. The cycle is divided into four different phases: G1 phase, S (synthesis) phase, G2 phase and M (mitosis) phase, where G1/S/G2 corresponds to interphase.

In S phase the nuclear DNA is replicated which leads to the doubling of genetic information. During M phase, the process of nuclear division, chromosomes are partitioned into two daughter cells. The remaining phases G1 and G2 are gaps between mitosis and S phase. They provide time for the cell to grow and to double their mass of proteins and organelles. Under typical laboratory growth conditions the cell cycle of fission yeast has, in contrast to the human cell cycle, a short G1 and a long G2 phase. Cytokinesis occurs just after mitosis, as in human cells. However, because of the short G1, completion of cytokinesis in fission yeast coincides with the end of S phase under standard laboratory growth conditions.

The cell cycle is highly coordinated so that each stage occurs in a defined order and at the right time point. Key regulators are Ser/Thr-specific protein kinases

that trigger the transition between each cell-cycle phase. These protein kinases, also called cyclin-dependent kinases (CDK), phosphorylate and activate other enzymes and proteins important during the cell cycle. Since they are essential for the major cell-cycle transitions, their activity is tightly controlled. The cells employ three major strategies to regulate CDK activity.

- In order to be active CDKs have to complex with cylins.
  The expression level of the different cyclins rises and falls through the cell cycle, with different cyclins being expressed in different cell-cycle phases. This ensures that the right CDK activity is provided at the right time to the right level. Cdc2 is the only CDK in fission yeast. It associates with four different cyclins. The cyclin Cig2 complexes with Cdc2 in early G1 and remains bound until the end of S phase, Cig1 and Puc1 are associated with Cdc2 in late G1. The CDK-cyclin complex Cdc2-Cdc13 is present in S, G2 and M phase (Moser & Russel, 2000; Krohn *et al.*, 2008).

- Phosphorylation of the kinase component.
  Phosphorylation of the T-loop, a flexible region of the kinase, leads to a conformational change so that the loop no longer blocks the catalytic pocket of the kinase. This phosphorylation stimulates the kinase activity enabling the substrate to access the active site. On the other hand phosphorylations on other sites of the catalytic pocket can decrease substrate affinity. In fission yeast phosphorylation of the kinase Cdc2 at tyrosine 15 (Y15) inhibits its activity.

- CDK inhibitors (CDI) bind to the CDK and thereby rearrange the catalytic site to inhibit its function (Alberts *et al.*, 2008; Pollard *et al.*, 2007).

Cell-cycle regulation at the G2/M transition

At the beginning of G2 Cdc2 is already associated with Cdc13, the cyclin needed for entry into mitosis. To prevent cells from going into mitosis at this early stage the Cdc2-Cdc13 complex is kept inactive by an inhibitory phosphorylation on Cdc2 Y15. The phosphorylation is maintained by the kinases Mik1 and Wee1 during G2 until cells are ready for mitosis. At the G2/M transition the inhibitory phosphate is removed by Cdc25 which activates Cdc2 and triggers entry into mitosis (figure 2.1).

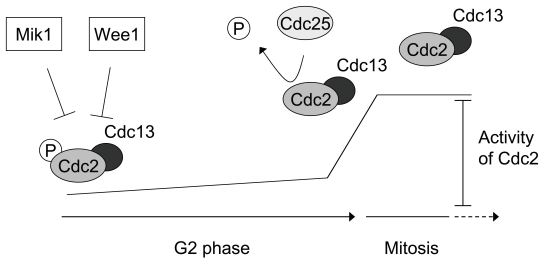

Figure 2.1.: Cell-cycle regulation in G2 phase and early mitosis. Activity of the CDK-cyclin complex Cdc2-Cdc13 is responsible for the G2/M transition (Moser & Russel, 2000).

2.4. Cell-cycle checkpoints

Checkpoints are control mechanisms that actively halt cell-cycle progression (Kastan & Bartek, 2004). In fission yeast several checkpoint pathways monitor the status of the DNA and arrest the cell cycle in response to DNA damage or inhibition of DNA replication. They include mechanisms to inhibit mitosis when the DNA is damaged (the G2/M checkpoint) or S phase is perturbed (the S/M checkpoint) as well as a mechanism to inhibit ongoing DNA replication when the DNA is damaged (the intra-S checkpoint). Other checkpoints relevant for this work are the G1/S checkpoint (see below) and the spindle assembly checkpoint. The spindle assembly checkpoint regulates transition from metaphase to anaphase and monitors tension and/or occupancy at the kinetochores (Lew & Burke, 2003). In the DNA-damage checkpoints pathways consist of sensor, mediator and effector components that transduce the checkpoint signal from DNA damage to an appropriate cell cycle response. At the end of the signaling cascade the CDK is inactivated by an inhibitory phosphorylation which leads to a cell-cycle arrest.

2.4.1. The DNA-damage checkpoint

In a log phase culture of fission yeast most cells will reside within G2 phase as it is the longest cell cycle phase. Therefore the G2/M transition is the major control point in fission yeast (Humphrey, 2000).

The first event in the checkpoint response is damage recognition. In the G2/M checkpoint this is executed by the *rad* checkpoint genes. There are two complexes that bind to damaged DNA independently of each other. This includes

the checkpoint proteins Rad3-Rad26 and the Rad9-Rad1-Hus1 complex, also called the checkpoint sliding clamp (CSC) due to its homology to the PCNA, the sliding clamp for the polymerase in DNA replication (O'Connell *et al.*, 2000). The CSC is loaded onto chromatin by yet another checkpoint rad protein, Rad17. Binding of Rad3 to damaged DNA induces phosphorylation of both Rad26 and the CSC. The mediator Crb2 serves as an adaptor protein between sensor and effector kinases (Kilkenny *et al.*, 2008). Crb2 is required for Rad3/CSC-dependent phosphorylation of the checkpoint effector kinase, Chk1, which also undergoes autophosphorylation and thereby amplifies the DNA damage checkpoint signal (Humphrey, 2000). Chk1 inactivates Cdc25 by an inhibitory phosphorylation and increases the activity of Wee1 by phosphorylation. Both phosphorylations lead to the accumulation of Cdc2 in its Y15-phosphorylated, inactive form and consequently to a cell cycle arrest (Figure 2.2).

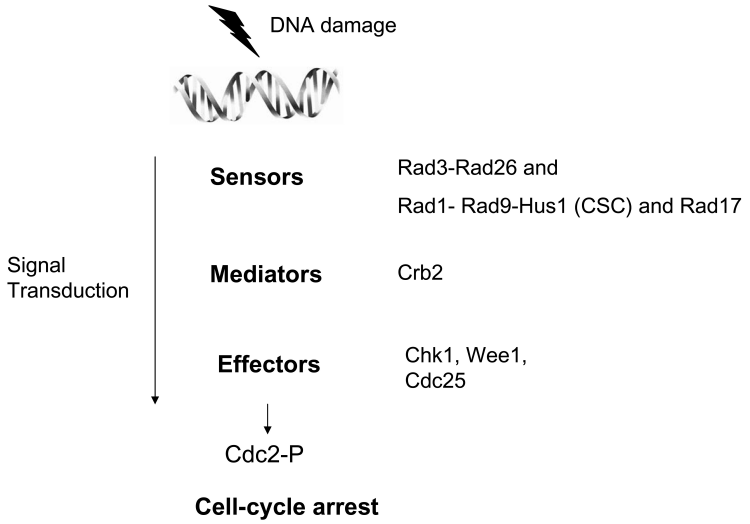

Figure 2.2.: The checkpoint response for the DNA damage checkpoint at the G2/M transition.

2.4.2. The G1/S checkpoint

The G1/S checkpoint in *S.pombe* is dependent on the kinase Gcn2 (Tvegard *et al.*, 2007). The Gcn2-dependent checkpoint can be activated by UVC, methyl methanesulfonate (MMS) and H_2O_2 and leads to inhibition of an early step in the preparation for S phase and thereby to a delay at initiation of DNA replication.

The only known substrate for Gcn2 is eIF2α, which is phosphorylated in response to UVC, MMS and H_2O_2 (Krohn *et al.*, 2008). Phosphorylation of eIF2α leads to a downregulation of general translation, although some selected mRNAs are still translated (Krauss, 2008). It is as yet unclear whether there is a causal relationship between translation downregulation and cell-cycle delay. It is conceivable that Gcn2 phosphorylates an unknown substrate that is required for entry into S phase. It is also possible that eIF2α phosphorylation and/or downregulation of translation is directly responsible for the cell-cycle delay, presumably by translational regulation of a protein required for entry into S phase.

It is not yet known what the signal is that activates Gcn2. UVC and the other agents cause DNA damage, as well as damage to RNA and proteins. It is not clear whether the signal derives from DNA damage or damage to other macromolecules. Gcn2 is known for its role in translation downregulation after starvation. In that case, it is activated by the accumulating uncharged tRNAs. It is not immediately obvious how UVC, MMS and H_2O_2 might lead to the accumulation of uncharged tRNAs (figure 2.3).

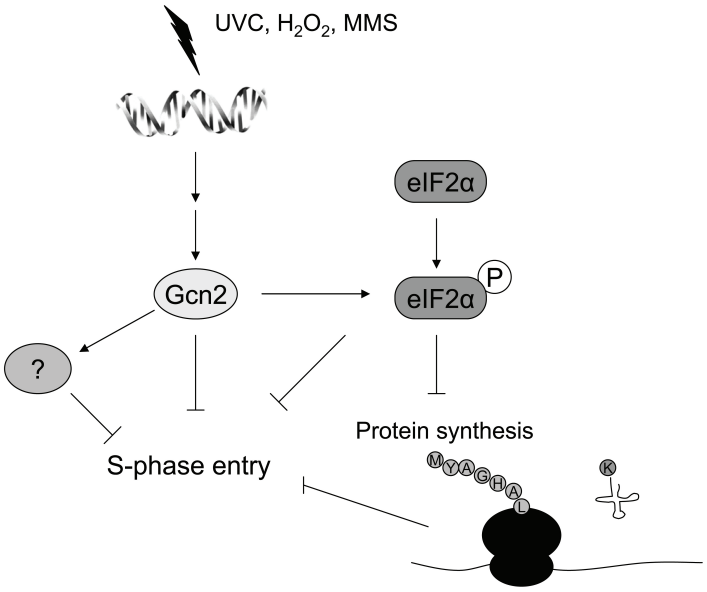

Figure 2.3.: The G1/S checkpoint model (Krohn *et al.*, 2008).

2.5. Gcn2, cell-cycle regulation and cancer

Cell growth and cell-cycle progression are tightly coupled processes (Fingar & Blenis, 2004; Petersen & Nurse, 2007). The cell has to increase in cell mass through biosynthesis of macromolecules to maintain cell size at division. Otherwise cells would get smaller with every cell cycle. Therefore cell growth requires a sufficient nutrient supply. As reviewed in Hinnebusch (2005) Gcn2 is a kinase which senses the availability of nutrients (amino acids) and is activated by uncharged tRNAs. It has also been reported that Gcn2 is activated by glucose deprivation. In this case activation is indirect and due to the fact that amino acids are used as a secondary energy source (Wek & Staschke, 2010).

It has been shown by Deng *et al.* (2002) that Gcn2 is activated by UVC light also in human cells, but it is not clear yet whether it is important for the regulation of G1/S in human cells. Given the observation that the activity of Gcn2 is important for the survival of cancer cells (Wek & Staschke, 2010; Ye *et al.*, 2010), it is all the more important to understand whether and how Gcn2 might regulate the cell cycle.

Chapter 3.

Aim of study

A novel checkpoint which is dependent on Gcn2 and inhibits entry into S phase after UVC irradiation in G1 was described by Tvegard *et al.* (2007). It could also be shown that Gcn2 is activated after UVC irradiation in G2 (Krohn *et al.*, 2008). This observation led to the question whether activation of Gcn2 after UVC irradiation in G2 has any effect on cell-cycle progression from G2 phase into mitosis. The aim of this study is to investigate the role of Gcn2 in the G2/M transition.

Chapter 4.

Materials

4.1. Yeast strains

The following S.pombe strains were used in this study.

Table 4.1.: *Schizosaccharomyces pombe*

Strain	Referred to as	Genotype	Source
489	wild type	*cdc10-M17 h-*	lab collection
1137	*gcn2*Δ	*gcn2::ura4+ cdc10-M17 ura4-D18 h+*	lab collection
1153	*rad3*Δ	*rad3::ura4+ leu1-32 ura4-D18 ade6-704 h-*	lab collection
1353	*rad3*Δ	*rad3::ura4+ cdc10-M17 ura4-D18 h+*	lab collection
1638	*gcn2*Δ *rad3*Δ	*gcn2::ura4+ rad3::ura4+ cdc10-M17 ura4-D18*	this study

4.2. Enzymes

Enzymes presented in table 4.2 were used for PCR, crossing of yeast strains, isolation of DNA and flow cytometry.

Table 4.2.: List of enzymes and their suppliers.

Enzyme	Supplier
High Fidelity Polymerase	Roche
Ribonuclease A	Sigma-Aldrich
S.H.P/H.P.J Helix Pomatia Juice (helicase)	BioSepra
Zymolase 20T	MP Biomedicals

4.3. PCR primers

Primers listed in table 4.3 were used for amplification of *gcn2* or *rad3*.

Table 4.3.: List of primers and primer sequences. Primers were delivered by Invitrogen.

Gene	Primer	Direction	Sequence
gcn2	*SP/BamHI_Gcn2_ ORF*	forward	5' TAGCGGATCCTAAAAGCTGTTCATGGAATGC 3'
	ASP/XmaI_ Gcn2_ ORF	revers	5' TAGCCCCGGGTTTAAGTCCATAAGATAAA 3'
rad3	*Rad3_sense*	forward	5' TATTTTTGACGTTTTGGACAGG 3'
	inura4rev2	revers	5' CCAGGATATGGTAGAAAAAC 3'

4.4. Antibodies

Primary and secondary antibodies used for immunoblotting and cell staining are presented in table 4.4 and 4.5.

Table 4.4.: List of primary antibodies and their suppliers.

Primary antibody	Supplier
Anti-cdc2-P antibody, rabbit	
Anti-tubulin antibody, mouse	
TAT1 antibody, mouse	

Table 4.5.: List of secondary antibodies and their suppliers.

Secondary antibody	Supplier
Cy3-linked antibody, Sheep anti-mouse, IgG	GE Healthcare
alkaline phosphatase-linked antibody, Goat anti-mouse, IgG + IgM (H+L)	GE Healthcare
alkaline phosphatase-linked antibody, Goat anti-rabbit, IgG + IgM (H+L)	GE Healthcare

4.5. Molecular weight standards

Molecular weight standards were used as a reference point to estimate DNA or protein size on an agarose or polyacrylamid gel. They are listed in table 4.6 and 4.7.

Table 4.6.: DNA standard and supplier.

DNA molecular weight standard	Range	Supplier
O'GeneRuler™1kb DNA ladder	0.25-10 kb	Fermentas

Table 4.7.: Protein standard and supplier.

Protein molecular weight standard	Range	Supplier
Dual Color Precision Plus Protein Standard	10-250 kDa	Bio-Rad

4.6. Chemicals and reagents

Chemicals and reagents used are presented in table 4.8.

Table 4.8.: List of chemicals and their suppliers.

Chemical	Supplier
DAPI (4,6-diamidino-2-phenylindole)	
Ethanol	Kemetyl Norge AS
Methanol	Merck
Phloxin B	
Sytox green	Invitrogen
Trichloroacetic acid (TCA)	

4.7. Solutions

4.7.1. Growth media and agar plates

Formulations of growth media and agar plates are detailed in table 4.9.

Table 4.9.: Yeast media and recipes.

Media	Recipe
YE 50 medium	17.625 g YE 50 (Sunrise Science products # 2009-500) to 500 ml H_2O, sterile filtrated
YE 50 agar	26,125 g agar powder (Sunrise Science products # 2010-500) to 500 ml H_2O, autoclaved at 121°C for 15 min
YE 50 agar with phloxin B	YE 50 agar supplemented with 5 mg/liter phloxin B
YE 50 agar with hydroxyurea (HU)	YE 50 agar supplemented with 15 mM HU
EMM medium	15.9 g EMM (Sunrise Science products # 2005-500) to 500 ml H_2O, sterile filtrated
EMM agar	24.4 g EMM agar (Sunrise Science products # 2006-500) to 500 ml H_2O.

4.7.2. Buffers and other solutions

Formulations of buffers and other solutions used in this study are presented in table 4.10.

Table 4.10.: Solutions and recipes.

Solution	Recipe
Agarose gel solution, 1%	1 % agarose 1 x TAE buffer
Citrate/phosphate pH 5.6	7.1 g/l Na_2HPO_4 11.5 g/l citric acid
Citrate/phosphate/EDTA/sorbitol	50 mM citrate/phosphate pH 5.6 40 mM EDTA pH 8.0

	1 M sorbitol
DTT, 1M	5g DTT 32.4 ml 0.01M NaAc
EDTA, pH 8.0 (0.5 M)	146,12 g/L EDTA NaOH to pH 8.0
Electrophoresis buffer, 10x	30,2 g/L tris 144 g/L glycine 1% (w/v) SDS
Lactose solution, 10%	10 g lactose 100 ml EMM
Lactose solution, 40 %	40 g lactose 100 ml EMM
Laemmli buffer, 2x	1.25 ml 1 M Tris HCl, pH 6.8 2.0 ml Glycerol 4.0 ml 10 % SDS solution 0.5 ml 0.1% (w/v) bromophenol blue 1 M DTT (final concentration 0.2 M) deionized H_2O to 10 ml
LiAc/TE, 10x	1 M lithium acetate 1x TE
PEG/LiAc/TE	40% PEG 4000 1x LiAc/TE
PEM	100 mM PIPES pH 6.9 1 mM EGTA 1 mM $MgSO_4$
PEMBAL	PEM 0.1 M L-lysine 1% BSA (globulin free) 0.1% NaN_3
Potassium acetate, 5 M pH 5	118 g KAc 46 ml acetic acid with acetic acid adjusted to pH 5

SDS, 20%	10 g SDS 50 ml H_2O
TBS-Tween	20 mM Tris HCl, pH 7.5 8 g/L NaCl 0.05% (v/v) Tween-20
TE, 10x pH 7.5	0.1 M Tris HCl pH 8.0 0.01 M EDTA pH 8.0 with HCl adjusted to pH 7.5
Transfer buffer	50 mM Tris base 380 mM glycine 0.1% (w/v) SDS 20% (v/v) methanol

Chapter 5.

Methods

5.1. Yeast media and cell handling

All media formulations are detailed in chapter 4.

Yeast extract medium (YE)
Yeast extract medium is a complete, rich but poorly defined medium which provides optimal growth conditions. When testing different genotypes YE medium was supplemented with phloxin B, a stain used to distinguish between dead and living yeast cells. Yeast cells growing on solid media containing phloxin B will range in color from light pink for living colonies to dark red for dead colonies (Kucsera *et al.*, 2000; Forsburg, 2003b). Hydroxy urea (HU) added to YE medium facilitated identification of HU sensitive mutants. HU inhibits the ribonuclease reductase and thereby depletes the supply of nucleotides. The checkpoint *rad* mutants are particularly sensitive to HU. They have a defective G2 arrest and will continue through the cell cycle despite incomplete replication due to the lack of nucleotides in S phase.

Edinburgh minimal medium (EMM)
A minimal medium contains only essential nutrient sources, salts and vitamins. In EMM all components are known and defined. It does not include any supplements and will therefore inhibit growth of mutants with auxotrophies (e.g. adenine, uracil). EMM was used when stable physiological conditions were needed as in experiments for cell-cycle progression.

Malt extract agar (MEA)
MEA is a complete, meagre, poorly defined medium. Cells growing on MEA soon run out of nutrients and, if cells of the opposite mating type are present, enter the

sexual differentiation pathway. MEA was used for conjugation and sporulation.

Storage of fission yeast

Yeast strains can be stored at -80°C. For this purpose a cell culture was grown to late-logarithmic phase and then mixed with 50% sterile glycerol in a 1:1 ratio. To reisolate cells, a small amount of the frozen glycerol stock is plated onto YE medium and incubated at 25°C.

Growth of liquid cultures

For physiological experiments (e.g. UVC irradiation) a fresh colony was inoculated in 10 ml YE medium and incubated at 25 °C until the next day (preculture). Cells from the preculture were transferred to liquid EMM and grown in log phase for 2 days at 25 °C. Exponential growth of the culture is obtained using the following equation for dilution from the preculture:

$$V_{preculture} = \frac{V_{total} \cdot OD_{desired}}{2^n \cdot OD_{preculture}} \qquad \text{and} \qquad n = \frac{t}{t_D} \tag{5.1}$$

where $V_{preculture}$ is the volume of the preculture used to inoculate, V_{total} is the total volume of the new culture, $OD_{desired}$ is the desired OD_{595} at a given time and $OD_{preculture}$ is the OD measured for the preculture. The number of generations n is defined by the time cells are grown in liquid medium t, divided by the doubling time of a given strain t_D.

5.2. Performing genetic crosses

In fission yeast conjugation and sporulation occur only when cells are starved for nutrients (Moreno *et al.*, 1991). MEA plates are usually used for genetic crossing. The two strains that are going to be crossed have to be of opposite mating type, h+ and h-. For crossing, a colony from each of the freshly plated strains was mixed and dissolved in 500 µl H_2O. 15 µl of the solution was then spotted onto MEA plates and left to dry. The cross was incubated at 25 °C for 2 days.

When asci could be seen under a light microscope (Zeiss, Germany), a colony with asci was resuspended in 500 µl H_2O. Then 5 µl helicase (Helix pomatia juice) was added and the mixture was incubated for 4 hours at 32 °C. The digestive juice of *Helix pomatia* is used to break down the cell wall of the asci and to kill vegetative

cells (Moreno *et al.*, 1991). Spores were plated out on YE agar and incubated at 25 °C until colonies formed.

5.3. Genomic Mini prep in *S. pombe*

For isolation of DNA from *S.pombe* a cell culture was grown to saturation in YE. Samples were prepared as follows:

1. The cell culture was centrifuged at 1100 x g for 5 min.
2. The pellet was washed once with ice cold water.
3. 1 ml citrate/phosphate/EDTA/sorbitol containing 2,5 mg zymolase was added for enzymatic digestion of the cell wall.
4. The suspension was transferred to an Eppendorf tube and incubated at 36 °C for 60 min. Spheroplasting was checked by adding 1 µl 10% SDS to 9 µl of the digested cells on a microscope slide.
5. Cells were then pelleted at 16 000 x g for 10 seconds The supernatant was removed and pellet resuspended in 500 µl TE.
6. 25 µl 20% SDS was added, the tube inverted several times and incubated at 65 °C for 1 h.
7. 175 µl 5 M potassium acetate (pH 5) was added, vortexed and kept on ice for 15 min.
8. After that the solution was centrifuged at 16 000 x g for 10 min at 4 °C.
9. The supernatant was carefully transferred to an other Eppendorf tube
10. 500 µl ice-cold isopropanol was added followed by mixing and another centrifugation step; 16 000 x g for 10 min at 4 °C.
11. The supernatant was removed and the pellet was washed with 500 µl 70% EtOH.
12. The pellet was air-dried over night and then resuspended in 40 µl TE
13. To confirm successful DNA extraction, 5 µl sample was analyzed by gel electrophoresis.

Purified DNA was stored at -20 °C.

5.4. Polymerase Chain Reaction (PCR)

Polymerase chain reaction is a technique used to amplify a specific DNA sequence from genomic DNA in a simple enzymatic reaction. The major components in a PCR are a heat-stable DNA polymerase, 2 oligonucleotide primers, a DNA template and deoxynucleotide triphosphates (dNTPs), in an appropriate buffer that ensures optimal enzyme activity. For the generation of primers it is important to know the sequence of interest as each primer is complementary to the respective end of the DNA sequence. In a PCR one amplification cycle consists of 3 steps: DNA denaturation, primer annealing and DNA synthesis.

In the first step (denaturation), DNA is separated into single strands by heat (94-95 °C). Then the temperature is lowered to allow annealing of the two primers to their complementary sequences in the template. Finally, primers are elongated by DNA polymerase synthesizing new DNA duplexes. A PCR usually consists of a series of 30-40 cycles which results in an exponential amplification in the amount of the chosen DNA sequence (Fletcher *et al.*, 2007; Berg *et al.*, 2007).
For all PCR reactions the High Fidelity PCR Master kit was used.

Polymerase Chain Reaction of *gcn2*
Primers used for amplification of *gcn2* were *SP/BamHI gcn2 ORF* and *ASP/XmaI gcn2 ORF*(see Chapter 4 - Materials: table 4.3). The primers are sequence-specific for *gcn2* and give PCR products for both *gcn2* deletion and *gcn2* wild type.

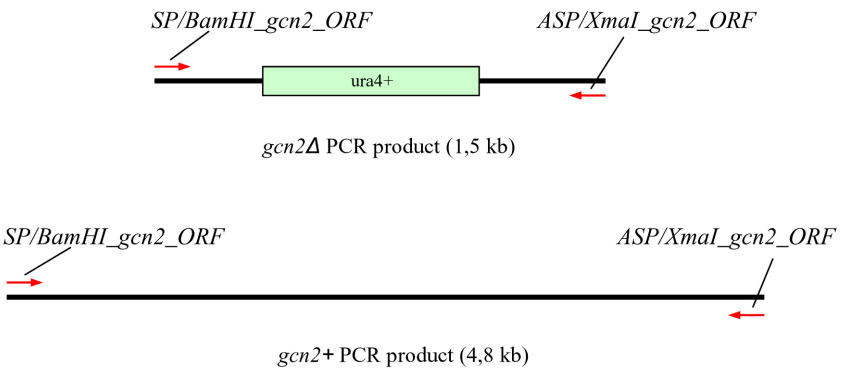

Figure 5.1.: Primers used for amplification of *gcn2*.

The reaction was run on a thermal cycler (Mastercycler ® gradient, Eppendorf, Hamburg, Germany). PCR conditions are outlined in figure 5.2. The PCR product was analyzed by gel electrophoresis.

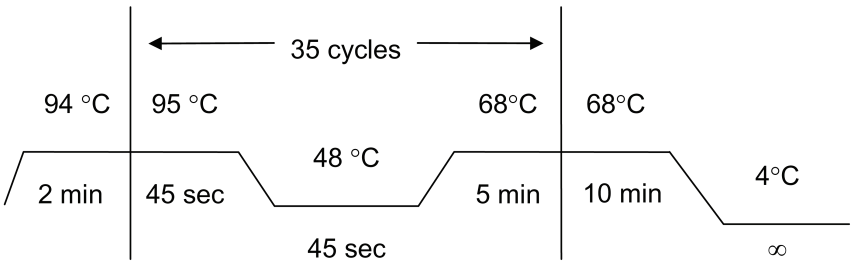

Figure 5.2.: PCR conditions for *gcn2* amplification.

Polymerase Chain Reaction of *rad3*

Primers used to confirm the *rad3* deletion were *Rad3_sense* and *inura4rev2* (see Chapter 4 - Materials: table 4.3). *Rad3_sense* is specific for the *rad3* gene, *inura4rev2* anneals to the *ura4*-marker. Therefore only the *rad3* gene carrying the *ura4*-marker will give a PCR product. There is no product expected for wild type *rad3*.

The reaction was run on a thermal cycler (Mastercycler ® gradient, Eppendorf, Hamburg, Germany). PCR conditions are outlined in figure 5.4. The PCR product

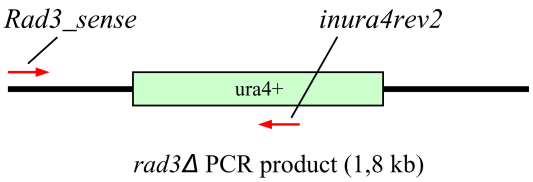

Figure 5.3.: Primers used for amplification of *rad3*.

was analyzed by gel electrophoresis.

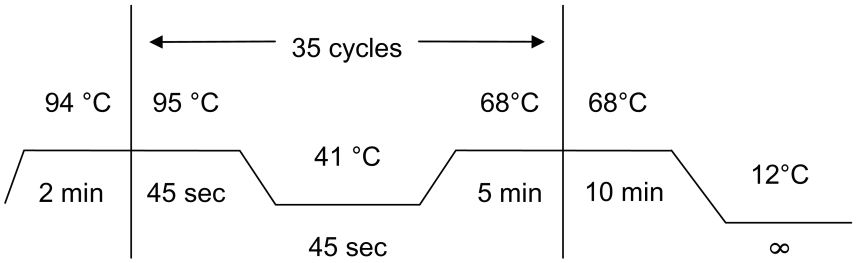

Figure 5.4.: PCR conditions for *rad3* amplification.

5.5. Synchronization methods

Synchronization is an important tool when analyzing cell-cycle progression since cells in a synchronous culture are dividing at the same time (Walker, 1999). There are several different synchronization methods to promote synchrony in an otherwise randomly dividing yeast population. In this study two different methods for synchronization were used.

The induction method of synchronization

One particular induction method is block and release of cdc mutants. In this study, synchrony was achieved using temperature sensitive *cdc10-M17* mutants. In *S. pombe* Cdc10 is a transcription factor required for expression of transcripts in G1. Incubation of $cdc10^{ts}$-cells at the restrictive growth temperature (36°C) blocks cell-cycle progression at the G1 stage (Sabatinos & Forsburg, 2010). Releasing the cells from temperature block results in a synchronous G1 culture.

In the current experiments, cells were grown to an OD=0.15 in minimal medium

at 25°C, then shifted to 36°C for 4h to arrest them in G1, then returned to 25°C to release them into the cell cycle (figure 5.5).

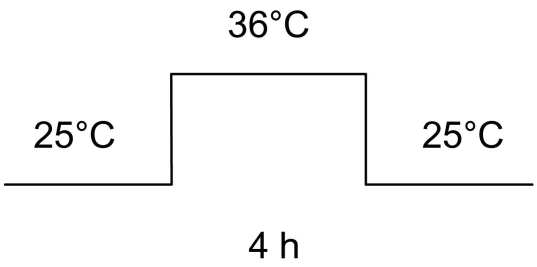

Figure 5.5.: Synchronization by block and release. Temperature sensitive *cdc10* mutants were incubated for 4 h at the restricted temperature to give a synchronous G1 culture.

The selection method of synchronization

Another method to synchronize a population of cells uses a sugar gradient to separate cells according to their size. Since fission yeast cells are very regular in size, selection of the smallest cells in a population results in a synchronous G2 culture. The sugar of choice for gradient-based synchronization of fission yeast cells is lactose because it cannot be metabolized by fission yeast and will therefore not perturb growth. The gradient was established using a gradient maker with a 10% and a 40% lactose solution (see materials for recipe).

There were always two consecutive gradients applied to achieve the best result for separation. Cultures were grown to mid-log phase, then loaded onto the gradient at a cell concentration of $5x10^9$/ml. The protocol used for lactose gradient synchronization is outlined below.

1. 500 ml cell suspension (OD_{595}= 0,5) was centrifuged for 3 min at 1100 x g.
2. The pellet was resuspended 5 ml YE medium.
3. 5 ml cell suspension was added onto the first gradient by pipetting along the inside of the tube.
4. The gradient with the applied cell suspension was then centrifuged for 3 min at 230 x g.
5. Afterwards 6 aliquots á 1 ml were collected from the top of the gradient.

6. To remove the remaining lactose in the collected suspension it was spun down at 1100 x g for 3 min and resuspended in 1 ml EMM.
7. 1 ml of the collected and resuspended suspension was added onto the second gradient similar to the first one by pipetting carefully along the inside of the tube.
8. The gradient with the applied cell suspension was then centrifuged for 3 min at 230 x g.
9. 500 µl aliquots were collected from the top of the second gradient; in total 6 aliquots each in seperate Eppendorf tube.
10. Synchrony was checked under the microscope. For good synchrony the cell size should be uniform and there should not be any cells with septa because septated cells are not in G2 but in G1 or S phase.
11. Cells from aliquots with the best synchrony were spun down at 1100 x g for 3 min to remove excess lactose and resuspended in 30 ml EMM.

5.6. UVC irradiation

In all experiments irradiation was done in G2 phase.

A suspension of synchronous cells was poured into a Petri dish to cover the bottom with a thin layer (3 mm). The cells were stirred while they were irradiated with 254 nm UVC light. The dose given was 1100 J/m^2 in about 3 min measured with a radiometer (UVCP, Upland, CA, USA). Samples were taken immediately after irradiation and then every 15 min.

5.7. Flow cytometry

Flow cytometry is a technique which facilitates analysis of DNA content in yeast cells. Analysis was performed with a BD™LSR II Flow Cytometer with 488-nm excitation light. Collected samples were prepared as follows:

1. 1 ml of cell suspension was spun down at 16 000 x g for 2 min, the supernatant removed and cells fixed in 1 ml ice-cold 70% EtOH on a vortexer.(Samples can be stored in the refrigerator.)

2. 500 µl of the sample was spun down at 16 000 x g for 2 min
3. The pellet was resuspended in 1 ml 20 mM EDTA and spun down at 16 000 x g for 2 min twice.
4. The supernatant was discarded and pellet resuspended in 500 µl 20 mM EDTA containing 100 µg/ml RNase A.
5. Samples were incubated over night at 36 °C.
6. Finally 500 µl 20 mM EDTA containing 2 µM Sytox Green was added.
7. Before running the flow cytometer samples were sonicated for 5 min and transferred to 5 ml tubes.

LSR II Flow Cytometer was run as described in the core facility manual. Analysis was performed as in Knutsen *et al.* (2011). This new method enables separation between mononuclear and binuclear cells by measuring the width as well as the total area of the DNA signal. Fluorescently labeled DNA remains in the excitation focus for a longer period of time when there are two separated nuclei than when there is only one nucleus in the cell. Therefore, the DNA signal (DNA-W) is expected to last longer for a binuclear than for a uninuclear cell (see figure 5.6 Panel C-E versus F-K). We also showed that by employing light-scatter measurements it is possible to exclude cell doublets(figure 5.6 Panel, and L-N) Binuclear cells were gated using the flow cytometry software to estimate the relative amount of binuclear cells (the binuclear index, BI).

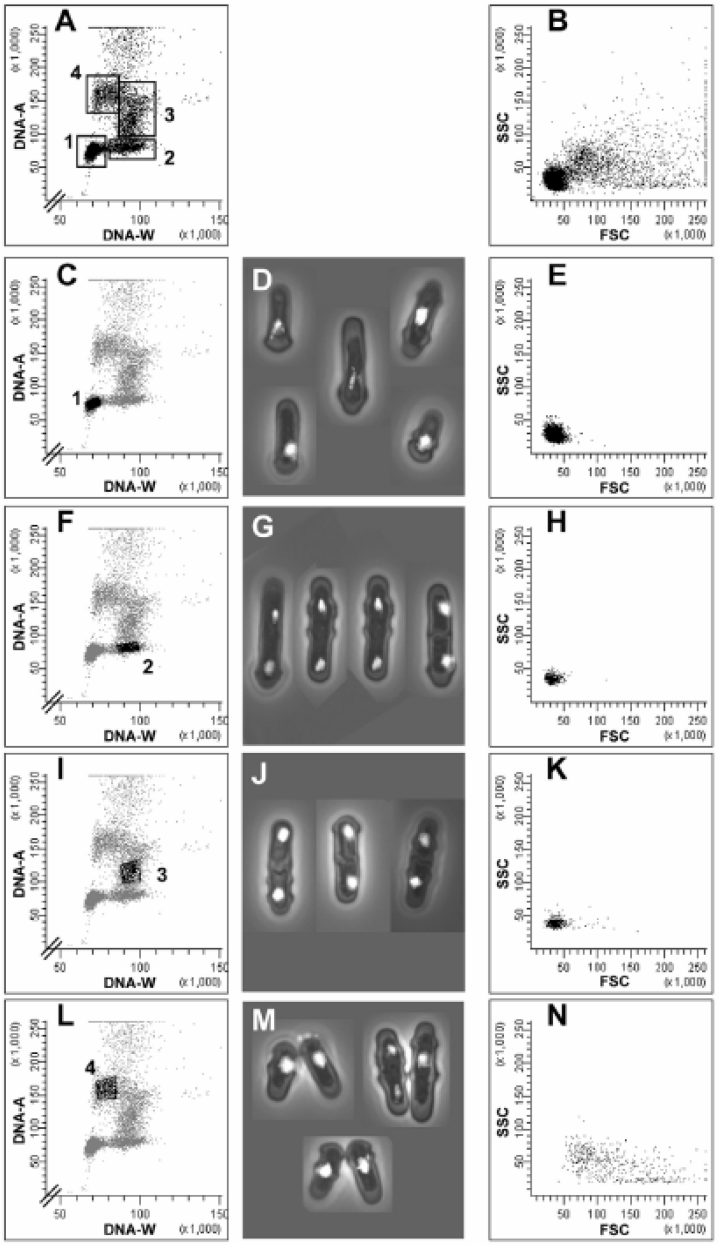

Figure 5.6.: Analysis of exponentially growing cells. Flow cytometric and microscopic analyses of wild-type S. pombe cells in an exponentially growing culture. First column: cytograms showing DNA-W versus DNA-A; second column: microscopy images of the sorted cells; third column: cytograms showing FSC versus SSC. The two-parametric DNA-A/DNA-W cytograms show four main subpopulations of cells: **1** G2 cells with a single nucleus and a 2C DNA content, **2** cells in G1 phase or late in mitosis with two nuclei and 2x 1C DNA content, **3** cells in S phase, with a DNA content between 2C and 4C, **4** cell doublets. From Knutsen *et al.* (2011).

5.8. Cell staining

Cell-cycle progression was not only monitored by flow cytometry but also by two different staining techniques: Staining of nuclear DNA or septa with fluorescent dye (4',6-diamidino-2-phenylindole (DAPI) and aniline blue, respectively) and staining of tubulin with a fluorescently-labeled antibody. The two dyes staining DNA and tubulin, visualize cellular structures (nucleus and mitotic spindle, respectively) that specifically enable determination of the number of cells in mitosis. Septated cells, determined by aniline blue staining are an index of cells in G1/S phase.

DAPI staining
Samples were fixed in 70% ice-cold EtOH, rehydrated and stained with DAPI to visualise chromosomes under a fluorescence microscope. Cells in mitosis show to distinct sets of chromosomes in the same cell. A detailed procedure of how samples were prepared for DAPI staining is outlined below.

1. 1 ml of an early-mid log phase culture was spun down at 16 000 x g for 2 minutes, the supernatant removed and cells fixed in 1 ml ice-cold 70% EtOH on a vortexer.

2. 500 µl of EtOH fixed cells was spun down at 16 000 x g for 2 minutes. The supernatant was discarded and pellet resuspended in 20 µl H_2O.

3. 5 µl suspension was placed onto a microscope slide and allowed to dry. A cover slip with 2,5 µl DAPI in 50% glycerol was applied.

Samples were observed with a fluorescence microscope (Leica DM6000B, Wetzlar, Germany) with 63x magnification. The MI was determined counting those cells that had two discernable nuclei but no septum.

Staining with aniline blue
Aniline blue stains the septum and was used to monitor the frequency of septated cells (septation index). A septum appears after nuclear division and is normally located at the midpoint of the newly divided cell. The procedure for staining with aniline blue is as for DAPI staining. Samples were fixed in 70% EtOH.

1. 1 ml of cell suspension was spun down at 16 000 x g for 2 minutes, the supernatant removed and cells fixed in 1 ml ice-cold 70% EtOH on a vortexer.

2. 500 µl of EtOH fixed cells was spun down at 16 000 x g for 2 minutes. The supernatant was discarded and pellet resuspended in 20 µl H_2O.

3. 5 µl suspension was placed onto a microscope slide and allowed to dry. A cover slip with 2,5 µl aniline blue was applied.

Samples were observed with a fluorescence microscope (Leica DM6000B, Wetzlar, Germany) with 63x magnification. The septation index (SI) was determined counting cells with a septum (Figure 5.7).

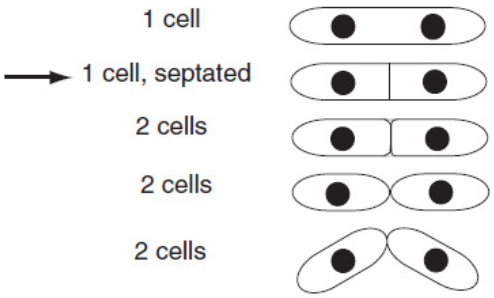

Figure 5.7.: Determining the frequency of septated cells. From Forsburg (2003a).

Immunostaining with anti-tubulin antibodies

β-tubulin is the major component of microtubules. Stained with a fluorescently-labeled anti-tubulin antibody it is possible to distinguish mitotic cells from interphase cells, based on their structural differences between interphase and mitotic microtubules (figure 5.8). Immunostaining with anti-tubulin antibodies and counting cells with a mitotic spindle provides another method to determine the MI.

For tubulin staining 10^8 cells were harvested for each sample. Samples were fixed in methanol (MeOH) prior to immunofluorescence labeling. A description of the procedure is outlined below.

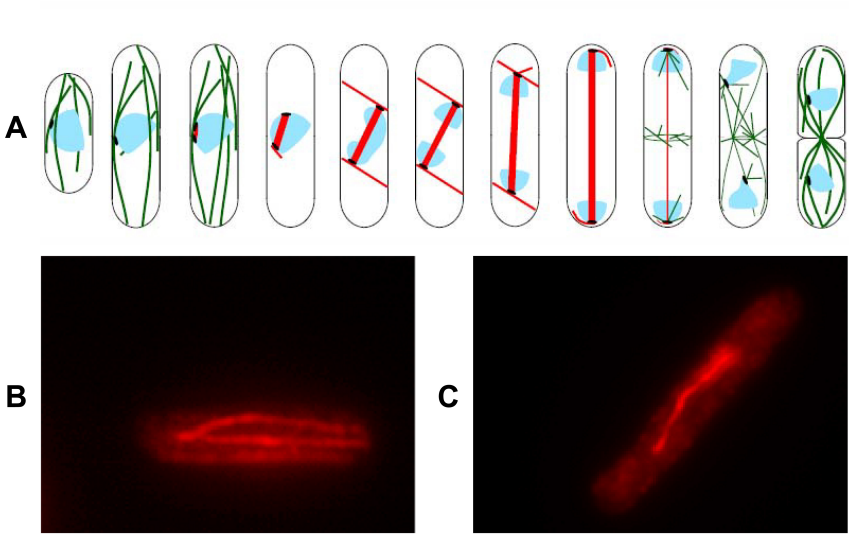

Figure 5.8.: Panel A: Schematic drawing of microtubule organization during the cell cycle. Interphase microtubules (green) are distributed throughout the whole cell. Mitotic microtubules (red) form a spindle with a single microtubule (Hagan, 1998), **Panel B and C:** Microtubules in interphase and mitosis (anaphase), respectively, stained with anti-tubulin antibodies (63x magnification).

1. Each sample was spun down at 1100 x g for 3 min and the supernatant was removed thoroughly.

2. Cells were fixed by adding 15 ml ice-cold MeOH.

3. To prepare samples for immunostaining with anti-tubulin antibodies, cells were spun at 1100 x g for 8 min.

4. Cells were resuspended in 1 ml PEM and transferred to Eppendorf tubes

5. Then spun again at 6 000 x g for 1 min and resuspended in 1 ml PEM with 3 mg/ml Lysing enzyme and 1 mg/ml Zymolyase 20T.

6. Cells were incubated at 37 °C until ~80% cells were digested.

7. Afterward samples were washed with 1ml PEM, spun at 6 000 x g for 1 min and resuspended in 1 ml 1% Triton in PEM for 30 seconds.

8. Samples were spun again at 6 000 x g for 1 min and wash 3x in 1 ml PEM.

9. The volume of the final pellet was roughly assessed.

10. Cells were resuspended in 1 ml PEMBAL and a volume which will give a 20-30 µl pellet upon a subsequent spin was transferred to each of two Eppendorf tubes.

11. Samples were put on a rotating wheel for 60 min at room temperature and after that spun at 6 000 x g for 1 min.

12. Cells were resuspended in 100 µl primary antibody (1/10 TAT1 in PEMBAL - supplied by Keith Gull) and incubated 16 h at 4°C on a rotating wheel.

13. Cells were washed 3x in 1 ml PEMBAL.

14. Cells were resuspended in 50 µl CY3-linked anti-mouse secondary antibody (1:200 in PEMBAL) for 1-2 h at room temperature. Samples tubes were wrapped in foil to protect the fluorophore from light to avoid bleaching.

15. Subsequently samples were washed 3x in 1 ml PEMBAL.

16. Finally the pellet was resuspended in 100 µl PEMBAL and cells were mounted on PolyL-lysine coated cover slips.

17. They were dried on a heating block and a cover slip with 2,5 µl DAPI in 50% glycerol was applied.

Samples were observed under a fluorescence microscope with 63x magnification (Leica DM6000B, Wetzlar, Germany) immediately after preparation. The MI was determined counting those cells that showed a single microtubule structure.

5.9. Immunoblotting

The third method applied to monitor cell-cycle progression is immunoblotting. Immunoblotting can be used to monitor the presence of cell-cycle regulated proteins and/or their modified forms. Dephosphorylation of the checkpoint kinase Cdc2 triggers entry into mitosis. By comparing the presence of dephosphorylated Cdc2-Y15 in untreated and UVC-irradiated samples it is possible to distinguish G2-arrested and M-arrested cells. Immunoblotting consists of several steps. Those included snap-freezing of cells after sampling, extraction of proteins from frozen samples, separation of proteins by sodiumdodecyl sulphate polyacrylamid gel electrophoresis (SDS-PAGE), transferring proteins from gel to membrane (Western blotting) and finally immunodetection using protein-specific antibodies.

Each technique is outlined below.

Snap-freezing of protein samples
10^8 cells were harvested for each sample.

1. Each sample was spun down at 1 100 x g for 3 min (4 °C) and the pellet was resuspended in 1 ml H_2O.

2. The cell suspension was transferred to a 2 ml tube which was followed by another centrifugation step at 1 100 x g for 2 min (4 °C).

3. The supernatant was removed and the cell pellet was frozen in liquid N_2 (-196 °C) to stop all cellular processes immediately.

Samples were stored at -80 °C.

TCA protein extraction

1. The cell pellet was thawed at room temperature and resuspended in 300 µl of 20% trichloroacetic acid (TCA)

2. 500 µl glass beads was added.

3. The tube containing cells, TCA and glass beads was placed in the Ribolyzer and cells were lysed 3x 20 sec at 6.5 m/s until broken cells were seen under a light microscope.

4. 600 µl 5% TCA was added and mixed thoroughly.

5. The cell lysate was spun into a new tube as follows: the lid of the tube with protein sample and beads was punctured with a needle and placed on top of a 1.5 ml screw cap tube upside down. Both tubes were placed in a 15 ml Falcon tube (figure 5.9)

6. Samples were spun for 1 min at 1 100 x g to remove the cell lysate from the glass beads.

7. Following another centrifugation at 16 000 x g for 10 min the supernatant was discarded and the protein pellet resuspended in 200 µl sample buffer (1x Laemmli buffer + 200 mM Tris-HCl pH 8)

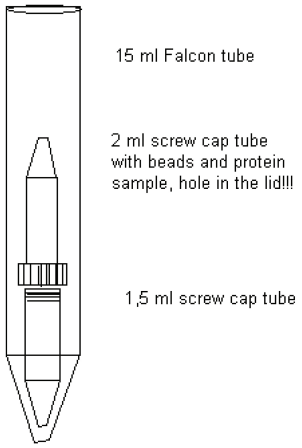

Figure 5.9.: Assembly of tubes to eliminate glass beads.

8. Boiled samples (heating block; 100 °C) were spun 1 min at 16 000 x g. The supernatant was transferred to a new tube and the pellet was discarded as it mainly contains unlysed cells.

Protein samples were frozen at -80 °C.

SDS-PAGE

SDS-PAGE is a qualitative method to analyze protein samples where proteins are separated based on their molecular weight. Proteins are dissolved in Laemmli buffer (sample buffer, see 9. under TCA protein extraction), which contains both dithiothreitol (DTT) that reduces disulfide bonds in the tertiary structure of proteins and SDS, an anionic detergent which denatures proteins. SDS binding unfolds polypeptide chains and confers a uniform negative charge per unit length. The migration of proteins is therefore dependent on their molecular weight rather than their intrinsic charge.

In preparation to SDS-PAGE, frozen protein samples were boiled in a heating block (100°C) to ensure total denaturation of the proteins. The gel was placed in a gel chamber filled with 1x running buffer and 10 µl samples were loaded onto the gel. The Precision Plus Dual Color was used as sizing marker (Appendix). Proteins were run on a polyacrylamid gel at 160 V for about 50 min. The current applied makes the negative charged protein-SDS molecules move towards the anode. Smaller molecules migrate faster than larger ones.

Western blotting

Western blotting is a technique where proteins separated by SDS-PAGE are transferred from the gel onto a membrane before reaction with antibodies. When an electrical current is applied negatively charged proteins migrate towards the positive pole. The current is applied at 90° to the gel. Therefore proteins will move out of the gel and onto the membrane (figure 5.10). A description of the procedure follows below.

For Western blotting an immuno-P membrane was prewet in 100% methanol and afterwards immersed in H_2O. The immuno-P membrane and the gel from the SDS-PAGE were soaked in transfer buffer for 5 min. Additionally two Whatman filter pads were soaked in transfer buffer for 10 min. Afterwards the mebrane sandwich was assembled as shown in figure 5.10 and air bubbles were removed with a pipette that was rolled over the membrane sandwich. A current of 15 V was applied for 45 min.

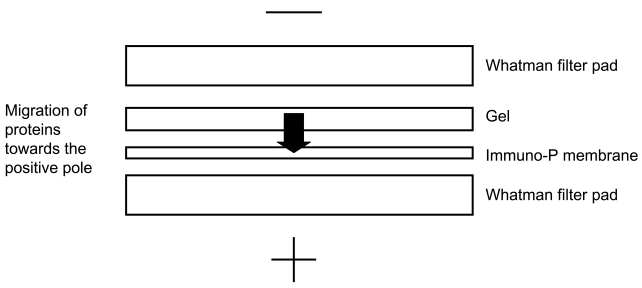

Figure 5.10.: Assembly of membrane sandwich for Western blotting

Immunodetection

After completing SDS-PAGE and Western blotting proteins on the membrane can be detected using antibodies. The membrane was incubated with a primary antibody that specifically binds the protein of interest. The primary antibody was detected by reaction with a second antibody conjugated to an enzyme which catalyzes a light-emitting reaction. In this study the enzyme linked to the secondary antibody was an alkaline phosphatase which dephosphorylates the ECF™ substrate to produce a fluorescent product.

The first step in immunodetection was to wash the membrane in 5 ml TBS-Tween for about 5 min at room temperature. Blocking was carried out in 5% dry milk

in TBS-Tween for 1 h. The membrane was incubated with the primary antibody (table 5.1) over night at 4°C.

Table 5.1.: Overview over primary antibodies used for detection of phosphorylated Cdc2p and tubulin

Primary antibody	Concentration	Protein size
Anti-cdc2-P antibody, rabbit	1:300	34 kDa
Anti- tubulin antibody, mouse	1:30 000	50 kDa

The antibody was removed and 3 consecutive washes were performed: 1x10 min and 2x5 min in 5 ml TBS-Tween. After that the membrane was incubated with the secondary antibody for 1 h at room temperature (table 5.2).

Table 5.2.: Overview over secondary antibodies which react with the primary antibodies

Secondary antibody	Concentration
Alkaline phosphatase, anti-rabbit	1:5 000
Alkaline phosphatase, anti-mouse	1:10 000

The secondary antibody was removed and 3 consecutive washes were performed: 1x10 min and 2x5 min in 5 ml TBS-Tween. Then the membrane was carefully drained for excess TBS-Tween on a paper towel and laid on a glass plate. 1-1,5 ml ECF™ was poured over the membrane and spread to cover it completely. The reaction was stopped when bands became visible but not later than 5 min and was then dried in the dark between two filter papers. Fluorescent bands appeared after exposure to 540 to 560 nm-light.
The membrane can be stored at 4°C covered in foil.

Chapter 6.

Results

In order to investigate the role of Gcn2 in the regulation of G2/M, we first constructed *gcn2 rad* double mutants and then followed their progression into M after UVC irradiation in G2.

6.1. Making *gcn2 rad3* double mutants

Table 6.1.: Parental strains used for crossing (1153 and 1137) and desired daughter strain (1638).

Strain	Referred to as	Genotype	Source
1153	*rad3*Δ	*rad3::ura4+ leu1-32 ura4-D18 ade6-704 h-*	Lab collection
1137	*gcn2*Δ	*gcn2::ura4+ cdc10-M17 ura4-D18 h+*	Lab collection
1638	*rad3*Δ*gcn2*Δ	*rad3::ura4+ gcn2::ura4+ cdc10-M17 ura4-D18*	This work

Deletion of *gcn2* alone was not expected to show any effect on cell-cycle progression after UVC irradiation due to activation of the powerful DNA damage checkpoint. Therefore a double mutant was produced crossing a *rad3*Δ mutant with a *gcn2*Δ mutant (see table 6.1). Possible effects of Gcn2 after UVC irradiation on cell-cycle progression could now be seen more easily.

When crossing the *rad3*Δ strain with the *gcn2*Δ strain, recombination can give 32 possible genotypes of the progeny. The 32 genotypes are due to five different genes: *rad3*, *gcn2*, *cdc10*, *leu1-32* and *ade6-704*. Each gene has two possible versions: wild type or mutated (2^5=32). Among the 32 possible genotypes there is just one that we are interested in and will employ: *rad3::ura4+ gcn2::ura4+ cdc10M-17 ura4-D18* (*rad3*Δ*gcn2*Δ mutant, see table 6. 1). The strategy used to

distinguish between the 32 genotypes was to grow them on appropriate media. By comparing growth on the different plates it was possible to limit the number of progeny whose genotype was further analyzed by PCR. All the possible genotypes and their growth characteristics on the employed selective plates are summarized in table 6.2. The rationale behind the selection strategy is given below.

After crossing, the spores were allowed to form colonies on YE plates at 25°C. For genotype testing colonies from a YE plate were replica-plated on the following media:

- EMM
  to identify *ura4+* colonies. This allows determination of progeny that has either the *gcn2*Δ or the *rad3*Δ or both.
- YEP+HU
  to identify the colonies that carry the *rad3*Δ. HU is an inhibitor of DNA synthesis (Enoch & Nurse, 1990; Elledge *et al.*, 1992) and leads to incomplete DNA replication. *rad* mutants are deficient in the S/M checkpoint and will continue into mitosis and cell division despite a defective S phase. Exposed to HU *rad3*Δ cells show aberrant mitosis and sometimes anucleated cells. When exposed to HU cells lose viability which leads to increased cell death (Alkhodairy & Carr, 1992). This means that *rad3+* grow in the presence of low concentrations of HU, while colonies with the mutated *rad3* are sensitive to HU and contain an increased number of dead cells. Phloxin B was used for better discrimination between dead and living cells and *rad3*Δ cells formed dark pink colonies and *rad3*$^+$-cells were pale pink.
- YEP, 36°C
  to identify *cdc10-M17* colonies. The *cdc10* mutation confers temperature sensitive growth. Cells with the temperature sensitive *cdc10* gene can not survive at restrictive temperature (36°C), while wild type cells do. Also here phloxin B was used for easier discrimination of dead and living cells.

In summary, by comparing growth on the three different media, colonies that grew on EMM but not on YEP+HU or on YEP + 36°C were picked. As shown in table 6.2 this leaves just 2 out of 32 genotypes possible for the picked colonies. For further identification, the genotype of these colonies was determined by PCR.

Table 6.2.: The table shows growth of progeny on different media. There are 32 possible genotypes from this cross. Growth on EMM and YEP supplemented with hydroxyurea at 25°C and on YEP at 36°C characterizes the genotype.

Genotype	EMM	HU	36°C
rad3::ura4+ leu1-32 ura4-D18 ade6-704			x
rad3::ura4+ ura4-D18 ade6-704			x
rad3::ura4+ leu1-32 ura4-D18			x
rad3::ura4+ ura4-D18	x		x
rad3::ura4+ leu1-32 ura4-D18 ade6-704 cdc10M-17			
rad3::ura4+ ura4-D18 ade6-704 cdc10M-17			
rad3::ura4+ leu1-32 ura4-D18 cdc10M-17			
rad3::ura4+ ura4-D18 cdc10M-17	x		
gcn2::ura4+ leu1-32 ura4-D18 ade6-704		x	x
gcn2::ura4+ leu1-32 ura4-D18		x	x
gcn2::ura4+ ura4-D18 ade6-704		x	x
gcn2::ura4+ ura4-D18	x	x	x
gcn2::ura4+ leu1-32 ura4-D18 ade6-704 cdc10M-17		x	
gcn2::ura4+ leu1-32 ura4-D18 cdc10M-17		x	
gcn2::ura4+ ura4-D18 ade6-704 cdc10M-17		x	
gcn2::ura4+ ura4-D18 cdc10M-17	x	x	
gcn2::ura4+ rad3::ura4+ leu1-32 ura4-D18 ade6-704			x
gcn2::ura4+ rad3::ura4+ura4-D18 ade6-704			x
gcn2::ura4+ rad3::ura4+ leu1-32 ura4-D18			x
gcn2::ura4+ rad3::ura4+ura4-D18	x		x
gcn2::ura4+ rad3::ura4+ leu1-32 ura4-D18 ade6-704 cdc10M-17			
gcn2::ura4+ rad3::ura4+ura4-D18 ade6-704 cdc10M-17			
gcn2::ura4+ rad3::ura4+ leu1-32 ura4-D18 cdc10M-17			
gcn2::ura4+ rad3::ura4+ura4-D18 cdc10M-17	x		
leu1-32 ura4-D18 ade6-704		x	x
leu1-32 ura4-D18		x	x
ura4-D18 ade6-704		x	x
ura4-D18		x	x
leu1-32 ura4-D18 ade6-704 cdc10M-17		x	
leu1-32 ura4-D18 cdc10M-17		x	
ura4-D18 ade6-704 cdc10M-17		x	
ura4-D18 cdc10M-17		x	

6.1.1. Polymerase Chain Reaction (PCR) of *rad3* and *gcn2*

To further investigate the genotype of progeny from the *gcn2*Δ x *rad3*Δ cross, candidates with a potential *rad3*Δ*gcn2*Δ genotype were picked and grown to saturation in liquid YE medium. Genomic DNA was isolated and two different PCRs were run, each with specific primers for either *rad3* or *gcn2* amplification. The PCR fragment of *rad3*Δ is expected to have a size of 1,8 kb while there is no product expected for the wild type of *rad3* (see Chapter 5 - Methods: figure 5.3). DNA from a *rad3*Δ strain was used as a positive control. In figure 6.1 bands

with the expected size for *rad3*Δ of 1,8 kb are observed for both candidates. In addition, the right product size is confirmed by the positive control of a *rad3*Δ mutant having a band of the same size. PCR of a wild type strain does not show any bands which eliminates unspecific binding of the primers. Together with the results from replica plating on YEP+HU, this confirms that both candidates carry a *rad3* deletion.

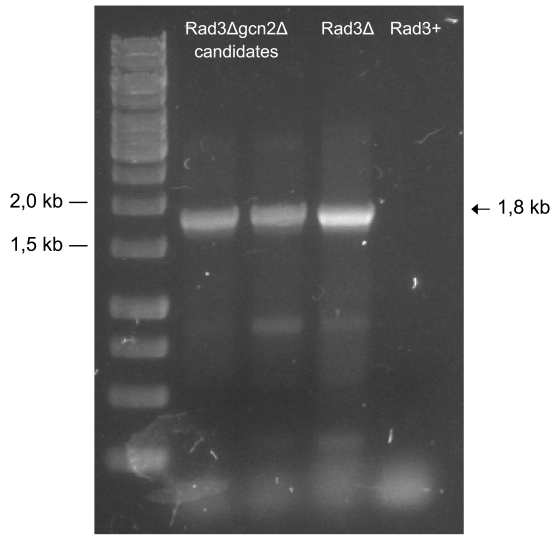

Figure 6.1.: Samples from putative *rad3*Δ*gcn2*Δ double mutants, positive control (*rad3*Δ) and negative control (*rad3*+).

Since there is no appropriate medium available to select for *gcn2* mutants, identification of *gcn2*Δ was done by PCR alone. The obtained band of 1,5 kb seen on the gel for *gcn2* PCR in figure 6.2 matches with the expected size of the *gcn2* deletion product (see chapter 5-Methods: figure 5.1). For comparison, the size of wild type *gcn2* is 4,8 kb. This suggests that candidates contain a *gcn2* deletion as well as a *rad3* deletion .

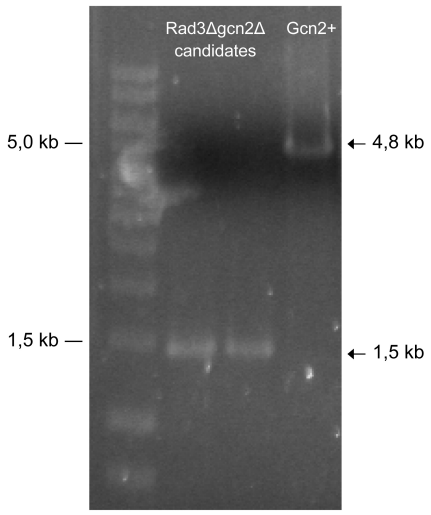

Figure 6.2.: Samples from putative *rad3*Δ*gcn2*Δ double mutants and negative control *gcn2*+.

Both candidates show PCR products with the right size for *rad3* and *gcn2* deletion and generation of a *rad3*Δ*gcn2*Δ double mutant is thereby confirmed. One of the two *rad3*Δ*gcn2*Δ double mutant was used in further experiments.

6.2. Measuring cell-cycle progression using *cdc10* block and release

We wished to compare the kinetics of entry into mitosis after UVC irradiation in *rad3*Δ*gcn2*Δ to that in *rad3*Δ cells. For this purpose cells had to be synchronized and then irradiated in G2 phase. Synchronization was achieved using *cdc10* block and release.

6.2.1. Cell-cycle analysis by flow cytometry

In order to follow cell-cycle progression, we used flow cytometry. Traditional flow cytometry analysis of the fission yeast cell cycle cannot distinguish between cells in G2, mitosis and G1 (2C versus 2x 1C). Therefore we have developed a new method (Knutsen *et al.*, 2011) that enables us to distinguish 2C cells with one nucleus (G2 and early M) from cells with two nuclei (anaphase - G1). In order to validate the new method, we have compared mitotic indices measured by flow cytometry and by traditional staining techniques. My major contribution to the paper was these comparisons in cdc10 block-and-release experiments (figure 5 in

Knutsen et al). The new method was used to first establish when the cells should be irradiated, then to follow entry into mitosis in wild type and mutant cells after UVC irradiation in G2.

6.2.2. Synchronization and timing of irradiation

Figure 6.3 below shows selected time points of *cdc10^{ts}* cells after release. The DNA histograms show DNA content on the x-axis with 50 as the value for cells with one copy of each chromosome and 100 as the value for cells with two copies of each chromosome.

71% of wild type cells and 92% of *gcn2*Δ cells arrested at the G1 stage when incubated at 36°C(panel A). 120 min after release from the temperature block the majority of cells in both strains have two copies (2C) of each chromosome (panel B). 150 minutes after release the population of binucleate cells (BI) increased to 8% in wild type cells and 23% in *gcn2*Δ cells (panel C), showing entry into mitosis. In the cytogram showing DNA content-W (DNA content-width) versus DNA content-A (DNA content areal) it can be seen that most of the cells are in G2. Hence, an incubation time of 4 h at 36°C is sufficient to induce a good synchrony in both strains.

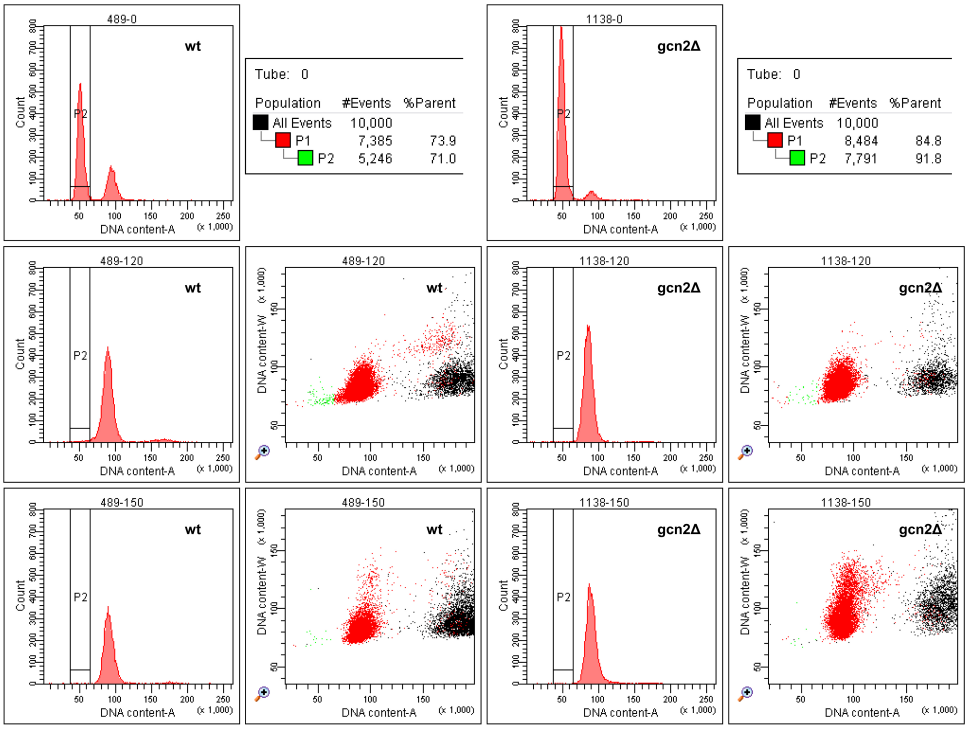

Figure 6.3.: Flow cytograms of wt (489) and *gcn2*Δ (1138) strain at time points 0, 120 and 150 min after release from the 4h-temperature block.

We monitored the frequency of binuclear cells (BI) as a function of time after shift down from the temperature block. Samples were taken for 195 min. Analysis by flow cytometry shows that the frequency of binuclear cells of wild type and *gcn2*Δ starts increasing at about 135 min after shift down from the temperature block (figure6.4). This means that by 135-150 min cells enter mitosis. It can be noticed that the *gcn2*Δ strain goes into mitosis faster than the wild type strain.

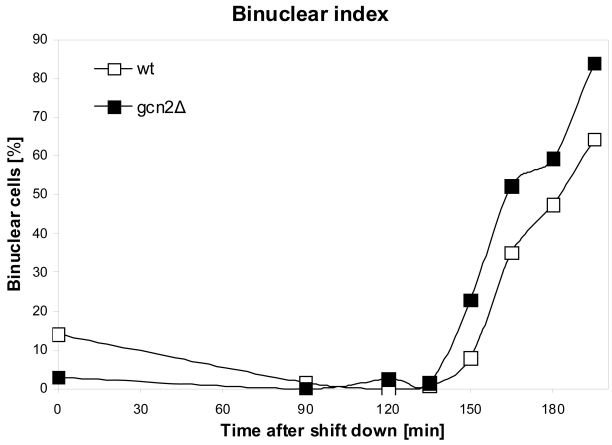

Figure 6.4.: Binuclear index (BI) of wt (489) and *gcn2*Δ (1138) strain monitored for 195 min after shift down from temperature block.

To confirm results measured by flow cytometry, the degree of synchrony was also analyzed using cell staining. Samples were taken as for flow cytometry but then stained with aniline blue to count septated cells. Septated cells appear concurrently with S phase and therefore later in the cell cycle than binuclear cells. Knowing that, the septation index can also be used to estimate entry into mitosis. In figure 6.5 wild type cells start septation at about 150 min after shift down. As seen for the BI in figure 6.4 *gcn2*Δ cells show septa earlier than the wild type, at about 135 min after shift down from the temperature block.

Based on the graphs for the binuclear and the septation index, cells enter mitosis between 135 min and 150 min after release from the temperature block. Therefore cells were irradiated approximately 110 min after shift down from the *cdc10* block to the permissive temperature to measure cell-cycle progression after UVC. At this time point both strains are still in G2 and we can expect that any G2/M

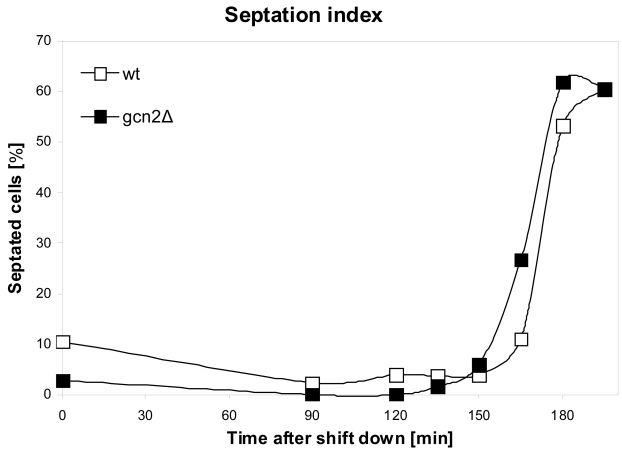

Figure 6.5.: Septation index (SI) of wt (489) and *gcn2*Δ (1138) strain monitored for 195 min after shift down from temperature block.

checkpoint would become activated upon irradiation.

6.2.3. Entry into mitosis after UVC irradiation

In this study cell-cycle progression of four different strains was compared (table 6.3).

Table 6.3.: Strains used in the experiments measuring cell-cycle progression.

Strain	Referred to as	Genotype	Source
489	wild type	*cdc10-M17 h-*	lab collection
1137	gcn2Δ	*gcn2::ura4+ cdc10-M17 ura4-D18 h+*	lab collection
1153	rad3Δ	*rad3::ura4+ leu1-32 ura4-D18 ade6-704 h-*	lab collection
1353	rad3Δ	*rad3::ura4+ cdc10-M17 ura4-D18 h+*	lab collection
1638	gcn2Δ rad3Δ	*gcn2::ura4+ rad3::ura4+ cdc10-M17 ura4-D18*	this study

Exponentially growing cdc10^{ts} cells were synchronized in G1 phase and exposed to UVC-light in G2 phase. After irradiation cell-cycle progression was measured by flow cytometry. Samples were taken immediately after irradiation and then every 15 min.

Analysis by flow cytometry (figure 6.6) shows that the frequency of binuclear cells increases in untreated samples after the time point of irradiation. All strains continue the cell cycle and enter mitosis as expected. By 75 min after the time of irradiation most of the untreated cells in all strains had passed mitosis having

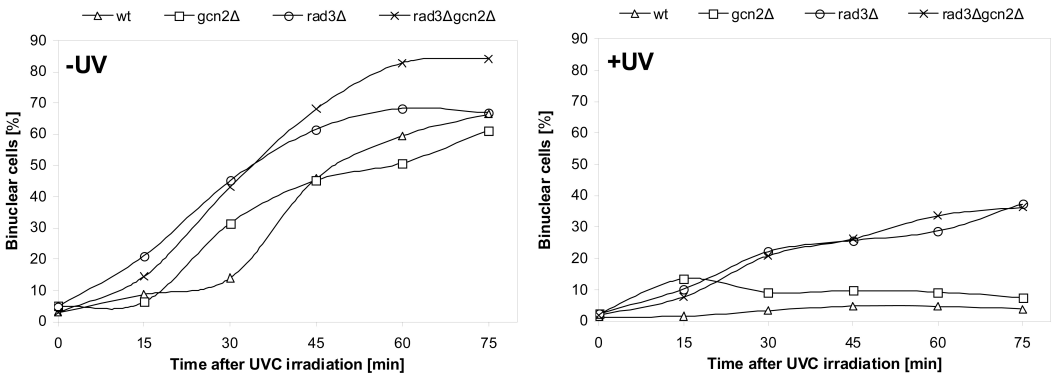

Figure 6.6.: Comparison of checkpoint response after UVC irradiation in wild type (wt), *gcn2*Δ mutant, *rad3*Δ mutant and *rad3*Δ*gcn2*Δ double mutant. The cells were synchronized by *cdc10* block and release and irradiated with UVC in G2.

more than 60% binuclear cells. When irradiated with UVC the frequency of binuclear cells of wild type and *gcn2*Δ cells does not increase significantly. The BI of both strains is below 15% throughout the whole experiment. We conclude that after treatment with UVC these two strains delay mitosis. The *rad3*Δ strain and the double mutant strain *rad3*Δ*gcn2*Δ show continous increase in the BI after UVC treatment. 75 min after irradiation about 40% of the cells had passed mitosis. The increase in binuclear cells of the *rad3*Δ and the *rad3*Δ*gcn2*Δ strain is significantly slower than in the untreated cultures. This result is surprising since the *rad3*Δ mutant is checkpoint deficient (Bentley *et al.*, 1996) and was expected to enter mitosis without any major delay.

6.2.4. Cell-cycle progression monitored by fluorescent microscopy

To further test the new flow cytometry-based method and confirm the conclusions drawn above, we monitored cell-cycle progression of two of the above strains (wild type and *rad3*Δ*gcn2*Δ) using a fluorescent staining technique. Samples were taken at the same time points as for flow cytometry but prepared for analysis with DAPI staining. Figure 6.7 shows the kinetics of entry into mitosis as measured by DAPI staining for UVC-treated and untreated samples of wild type and *rad3*Δ*gcn2*Δ strain. The frequency of mitotic cells determined using DAPI staining (mitotic index, MI) is compared with BI obtained using flow cytometry.

The graphs in figure 6.7 show that both methods to estimate number of mitotic cells give the same result. The wild type strain delays mitosis at least

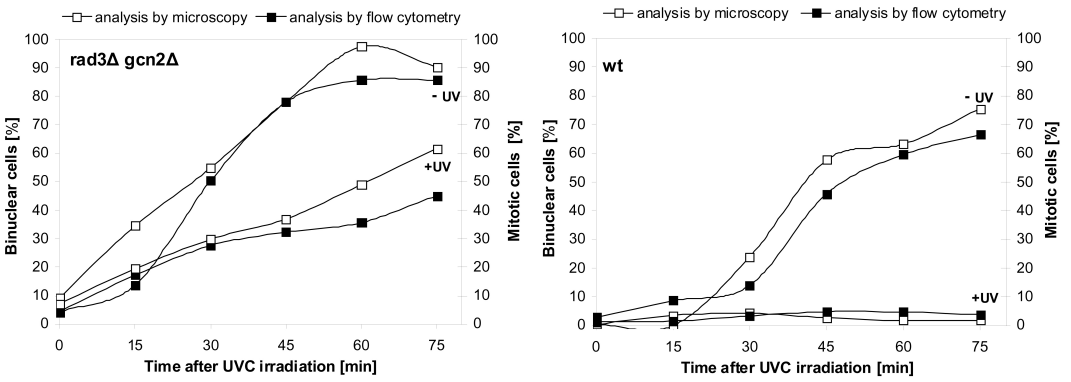

Figure 6.7.: Comparison of checkpoint response after UVC irradiation in wild type (wt) and *rad3*Δ*gcn2*Δ double mutant. The cells were synchronized using *cdc10* block and release and irradiated with UVC in G2. For graphs with open symbols binuclear cells were determined by DAPI staining, for closed symbols flow cytometry was used.

75 min after irradiation with UVC. The slow, gradual entry into mitosis of the *rad3*Δ*gcn2*Δdouble mutant is observed both when analyzing samples by flow cytometry and fluorescent microscopy.

We also employed immunofluorescent staining of β-tubulin as a third method to measure progression into mitosis. Here we compare entry into mitosis of wild type and *rad3*Δ.

In the beginning of mitosis the microtubules are reorganized to form the spindle apparatus which facilitates the distribution of the chromosomes to the daughter cells. We have stained β-tubulin using indirect immunofluorescence to visualize the microtubules. The mitotic spindle can be clearly distinguished from the interphase microtubule array (see methods). In the figure shown below the mitotic index was determined counting mitotic cells stained with a fluorescently-labeled tubulin antibody.

We found that already 35-40% of cells from *rad3*Δ-strain were in mitosis directly after irradiation. In contrast, there were only 0-5% mitotic cells observed in the wild type strain. The maximum of mitotic cells was reached 15 min after irradiation for the *rad3*Δ-strain, while wild type cells had a maximum of mitotic cell 45 min after irradiation. This indicates that cells with a *rad3* deletion complete S phase considerably earlier than wild type cells and were therefore irradiated when they had already passed any G2/M checkpoint. While the current

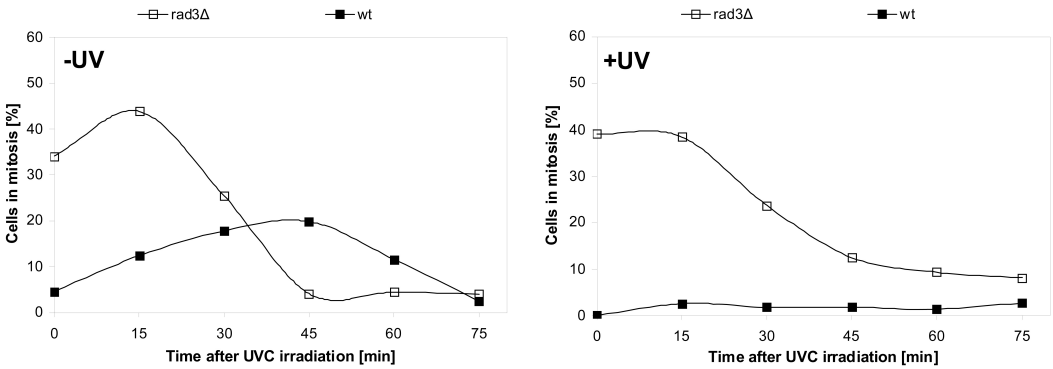

Figure 6.8.: Comparison of checkpoint response after UVC irradiation in wild type (wt) and *rad3*Δ mutant. The cells were synchronized using *cdc10* block and release and irradiated with UVC in G2. The MI was determined by counting cells with a mitotic spindle.

experiments were in progress, other results in the lab indicated that *rad3*Δ cells enter S phase earlier than the wild type cells after release from a *cdc10* block (Cathrine Arnason Bøe, personal communication). Therefore we decided to employ a selection synchronization method in further experiments.

6.3. Measuring cell-cycle progression using a selection method for synchronization

To further investigate cell-cycle progression of the *rad3*Δ strains we chose lactose gradient synchronization, a method which does not disrupt the cell cycle to the same extent as the induction method. This method is based on isolating the smallest cells from the population. Due to the short G1 (see Theoretical background 2.3), this results in a population of early-G2 cells. Therefore irradiation was performed immediately after synchronization.

6.3.1. Cell-cycle progression monitored by flow cytometry

As for cells synchronized with block and release, cell-cycle progression was monitored by flow cytometry to measure the frequency of binuclear cells. The binuclear index shows that all strains of the untreated samples have entered mitosis 30-45 min after the irradiation time point. Irradiated cells from all strains show a delay and do not enter mitosis until 75 min after irradiation with UVC. Consistent with the previous experiments using *cdc10* block and release, these

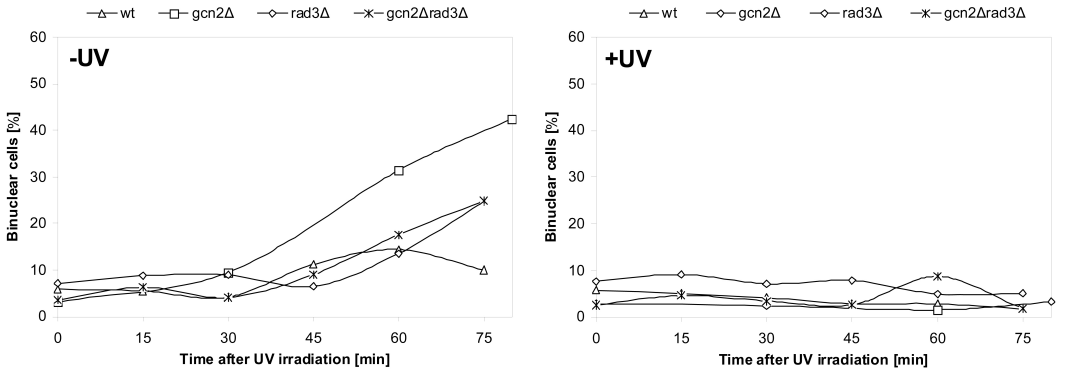

Figure 6.9.: Comparison of checkpoint response after UVC irradiation in wild type (wt), *gcn2*Δ mutant, *rad3*Δ mutant and *rad3*Δ*gcn2*Δ double mutant. The cells were synchronized by lactose gradient and irradiated with UVC in G2.

results indicate that Gcn2 does not have any effect on G2/M transition after UVC irradiation. Surprisingly, synchronized with the lactose gradient the *rad3*Δ strains showed a clear delay into mitosis, with the same kinetics as the wild type strain.

As Rad3 is an important component in the signaling pathway of the DNA damage checkpoint, a deletion of *rad3* was thought to result in a checkpoint-deficient mutant. Thus, the cell cycle delay of the *rad3*Δ strain upon UVC irradiation was unexpected in light of the general view in the field. We decided to pursue this observation and the main focus of this work shifted from exploring the role of Gcn2 to exploring the delay induced in the absence of Rad3.

6.4. The role of Rad3 after UVC irradiation

6.4.1. Confirming the *rad3*Δ strain

Having made the surprising observation that the *rad3*Δ strain delays mitosis after UVC irradiation, we considered the possibility that the strain has picked up a suppressor and/or there was a mistake in the main lab collection. First, we verified that the strain carries the *rad3*Δ by PCR. The strain clearly carries a deletion of *rad3*, since we could amplify the band specific for the deletion (figure 6.10).

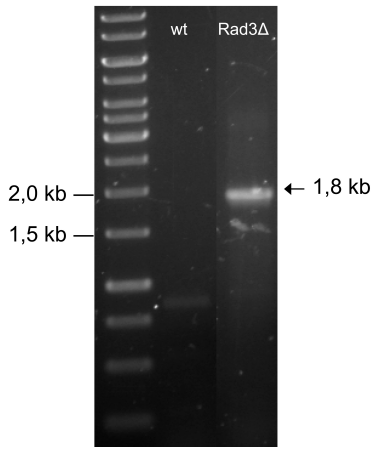

Figure 6.10.: PCR with *rad3*-specific primers (see Chapter 4 - Materials: table 4.3.)

Then we checked other, well-studied phenotypes of the *rad3*Δ mutant, namely entry into mitosis in the presence of HU and survival rates after UVC treatment. Consistent with the results of Bentley *et al.* (1996) we achieve a low survival of the *rad3*Δ strain when irradiating with a dose of 1 100 J/m^2 of UVC in G2. This dose gives a survival rate of 100% in the wild type strain, but only 7% in the *rad3*Δ strain (Gro Elise Rødland, personal communication).

After HU treatment, wild type cells arrest in early S phase and elongate. In contrast, the *rad3*Δ cells are known to enter mitosis with unreplicated chromosomes, which results in the so-called cut phenotype. As the cell tears apart unreplicated chromosomes, uneven chromosome segregation is typical for such mitoses. We compared wild type and *rad3*Δ cells after treatment with HU (figure 6.11). *rad3*Δ cells show newly divided cells with septa and a clearly visible cut phenotype. In contrast the wild type strain has elongated cells, arrested with only one nucleus after the HU treatment. Septa could not be observed in the wild type strain. We conclude that the *rad3*Δ strain is the right strain as judged by PCR and that it behaves as described in the literature after treatment with HU (Enoch *et al.*, 1992).

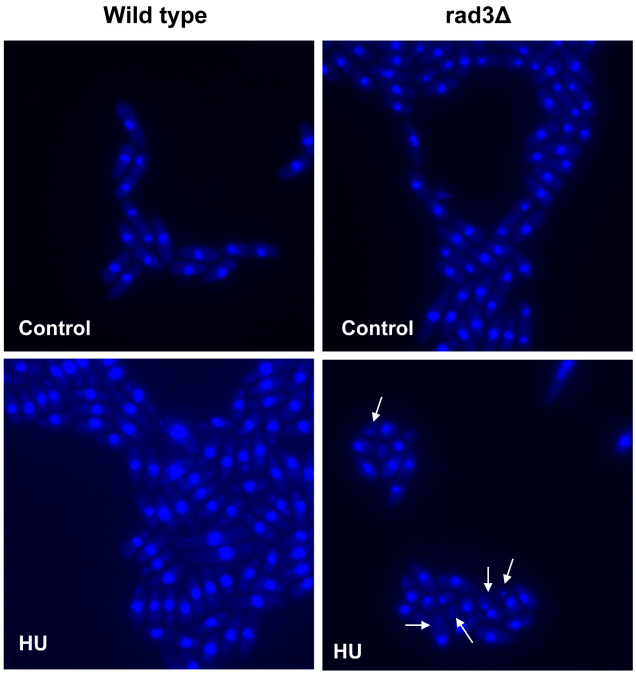

Figure 6.11.: Wild type and *rad3*Δ strain before and after HU treatment. Arrows show cells with the cut phenotype

6.4.2. Cell-cycle progression of *rad3*Δ monitored by immunoblotting

The binuclear index measures the number of cells in anaphase, G1 and S. It is therefore unclear whether the *rad3*Δ cells delay in G2 prior to entry into mitosis or in early mitosis, such as metaphase. In order to investigate more closely where in the cell cycle the *rad3*Δ cells delay, we followed the presence of the Y15 phosphorylated form of Cdc2 by immunoblotting, using a phosphospecific antibody. Dephosphorylation of Cdc2-Y15 is a hallmark event for entry into mitosis. Protein samples were taken at time points 0, 80 and 100 min after irradiation. Since lactose gradient synchronization only provides a limited amount of synchronous cells, it was not possible to take samples more often.

Cells of both strains, *rad3*Δ and wild type, show phosphorylated Cdc2-Y15 at time point 0 consistent with cells being in G2. We expected a decrease in the intensity of the phosphorylated Cdc2 band at 80 minutes, but this is difficult to see in this experiment. At 100 min after irradiation control samples show again phosphorylated Cdc2-Y15.

For samples irradiated with UVC, both *rad3*Δ and wild type show an increase in phosphorylated Cdc2-Y15 at 80 min compared to control samples suggesting that the cells arrest in G2 phase. At 100 min after UVC treatment the wild type strain shows Cdc2-Y15 phosphorylated suggesting a continued delay. Due to uneven loading it is difficult to conclude as to the length of the delay in the *rad3*Δ strain, but it appears somewhat less prominent than that in wild type cells.

From these rather preliminary results we conclude that the *rad3*Δ cells delay in G2 after UVC irradiation in early G2 in the same way as wild-type cells do, but the length of the delay might be somewhat shorter in the absence of Rad3.

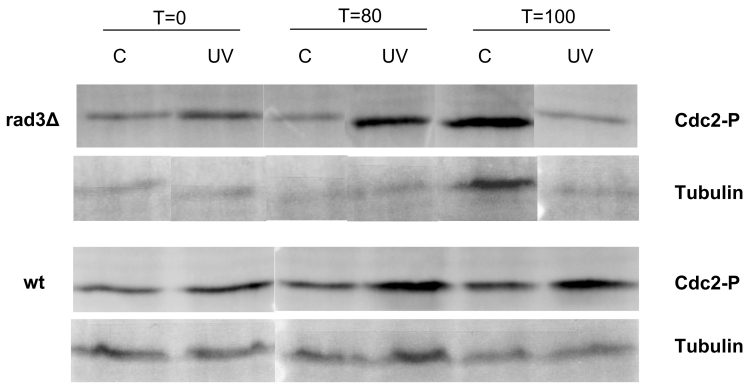

Figure 6.12.: Immunoblots probed with antibodies against phosphorylated Cdc2 and against tubulin as loading control showing samples from UVC irradiated wild type (wt) and rad3Δ mutant.

Chapter 7.

Discussion

Gcn2 and its role in the G2/M transition

In 2007 Tvegard *et al.* reported that UVC activated a Gcn2-dependent checkpoint in G1. Since activation of Gcn2 has also been observed in G2 phase (Krohn *et al.*, 2008) we investigated whether Gcn2 has any effect on cell-cycle progression from G2 phase into mitosis. In order to see a possible minor effect of Gcn2 on the G2/M transition, we constructed a *rad3*Δ*gcn2*Δ double mutant and monitored cell-cycle progression after UVC irradiation by flow cytometry to measure the frequency of binuclear cells. We have shown that the kinetics of entry into mitosis after UVC irradiation of *rad3*Δ and *rad3*Δ*gcn2*Δ cells were the same. This result is independent of the synchronization method we used (figure 6.9). Based on the literature and the general view in the field, we expected the *rad3*Δ strain to enter mitosis directly after irradiation with UVC in G2 but could not observe this when synchronizing with *cdc10* block and release. We suspected that the induction method we used might have affected the cell-cycle progression of the strains. Lactose gradient synchronization is a more gentle synchronization method and does not perturb cell-cycle progression to the same extent as synchronization with *cdc10*. Moreover this selection method was also used by Bentley *et al.* (1996) in their experiments characterizing Rad3. Therefore we decided to use lactose gradient synchronization in further experiments. However, the kinetics of entry into mitosis was similar between the *rad3*Δ and *rad3*Δ*gcn2*Δ strains also when lactose gradient centrifugation was used to synchronize the cells. While Gcn2 is clearly required for the G1/S checkpoint, we show here that it is not required for the regulation of G2/M after UVC irradiation.

The role of Gcn2 in the G1 phase is not totally elucidated yet. We know that it is required for translation downregulation and for the G1/S checkpoint response.

However, it is not clear if and how these two functions of Gcn2, translation downregulation and checkpoint activation, are connected and how they lead to the inhibition of S phase entry. One possibility is that Gcn2 acts directly on a cell cycle protein. In this scenario, Gcn2 might phosphorylate a G1-specific cell cycle protein. Alternatively, the effect on the cell cycle at G1/S might derive from Gcn2's effect on translation downregulation. In this scenario the difference between the roles of Gcn2 in G1 versus G2 might stem from different requirements for regulating translation of specific mRNAs that are necessary in G1 but not in G2.

Another observation was that the *gcn2*Δ mutant cells enter mitosis about 15 min earlier than wild type cells, using *cdc10* block-and-release (Fig 6.4-6.6). However, the early entry into mitosis is lost in irradiated *gcn2*Δcells (figure 6.6). It is difficult to find a plausible explanation for why the *gcn2*Δ enters mitosis earlier than the wild type strain, but it fits with our observation that under some growth conditions the *gcn2*Δ strain seems to have a slightly shorter generation time than the wild type strain (Beata Grallert, unpublished observation). As this enhancement of cell-cycle progression is clearly seen first when measuring the entry into mitosis but not in earlier cell cycle stages, one possibility is that the *gcn2*Δ mutant might be slightly faster in several or every cell cycle phase. We cannot exclude that Gcn2 has a subtle role also in the regulation of G2/M, but we can conclude that it has no major role in the regulation of G2/M after UVC irradiation in G2.

A Rad3-independent delay after UVC irradiation in G2

In the course of this work we observed that *rad3*Δ cells delayed mitosis in the same way as wild type cells do upon UVC-irradiation in G2 phase. We confirmed that this observation is made on a bona fide *rad3*Δ strain, which does have the deletion as judged by PCR. Our *rad3*Δ strain otherwise behaves as previously shown (Enoch *et al.*, 1992): it is sensitive to HU showing small septated cells with unevenly distributed chromosomes (cut phenotype) and has a low survival after UVC treatment. We therefore conclude that the *rad3*Δ strain is correct and that it did not pick up a suppressor.

This finding was most surprising as it contradicts the general view in the field that assumes that *rad3*Δ cells are checkpoint deficient after UVC irradiation.

This view is based on the findings of Bentley *et al.* (1996) who showed that *rad3*Δ mutants are checkpoint deficient after IR treatment and have low survival rates after UVC irradiation. To our knowledge checkpoint deficiency has not been shown after UVC irradiation, only generally assumed based on the profound UVC sensitivity and the established checkpoint deficiency after IR. As we show that *rad3*Δ cells do delay mitosis (either entry into or in early M, see below), we have to conclude that (i), an alternative pathway is activated that prevents mitosis in *rad3*Δ cells and (ii), Rad3 has an important, checkpoint-independent function(s) required for survival after UVC irradiation.

Cell-cycle progression measured by DAPI-staining and flow cytometry determines the frequency of cells that have entered anaphase since mitotic cells are first detected when chromosomes separate and two distinct nuclei appear. From those results we can therefore not conclude whether *rad3*Δ cells stand in G2 phase before entering mitosis or in metaphase in early mitosis. To investigate where cells arrest we employed immunoblotting to look at the phosphorylation state of Cdc2 after UVC irradiation in G2 since dephosphorylation of Cdc2 is a prerequisite for entry. We observed that at 80 minutes after irradiation Cdc2 accumulates in its phosphorylated form in both strains as compared to unirradiated control samples. At this time point *rad3*Δ cells show a clear arrest when monitoring cell-cycle progression with DAPI-staining and flow cytometry. This results indicate that cells are arrested in G2 rather than in metaphase. However, this experiment is hampered by technical difficulties in that we cannot obtain enough synchronous cells from lactose gradients to follow the kinetics of Cdc2 dephosphorylation more closely. Therefore further studies are needed to confirm this result. Another approach would be to identify mitotic cells by tubulin staining. If *rad3*Δ cells do not show the mitotic spindle after UVC irradiation, this would be another evidence for an arrest in G2 phase.

If the cell-cycle delay following UVC-irradiation is independent of Rad3, this raises the question which other proteins might be responsible for the delay.

In mammals two functionally distinct pathways depending on the type of DNA damage exist. Either of two protein kinases, ATM or ATR, initiates the signaling pathway (Alberts *et al.*, 2008). ATR, the human homolog of Rad3, is activated by UVC-induced DNA damage, while ATM, the human homolog of Tel1, plays an

important role after DNA double strand break. However, until now no checkpoint role of Tel1, the ATM homologue in *S.pombe*, has been described. So far the only known role of Tel1 is in telomere maintenance in fission yeast. To investigate the possible requirement for Tel1 in the G2 delay of *rad3*Δ cells, we are currently constructing a *rad3*Δ*tel1*Δ double mutant. cell-cycle progression of *rad3*Δ*tel1*Δ after UVC irradiation in G2 will give information about whether Tel1 is involved in a checkpoint.

Previously a study in budding yeast demonstrated that the role of Tel1 in checkpoint signaling is not limited to mammals (Clerici *et al.*, 2004). They showed that when *MEC1*Δ cells are irradiated in G1, they delay entry into mitosis. The delay depends on both Tel1 and components of the spindle assembly checkpoint (SAC). The activation of Tel1 in the absence of Mec1 led to the phosphorylation of the downstream effector kinase Chk1. Since activation of Tel1/ATM after DNA damage is observed in both human and budding yeast, Tel1 might have a role in checkpoint activation in *S.pombe* as well.

As for the requirements for the SAC after UVC irradiation in G1, it is important to note that budding yeast has the unique feature of assembling a short mitotic spindle already at the beginning of S phase. Thus irradiation in G1 might affect multiple components leading to activation of the SAC, possibly due to defects in the spindle pole body (SPB) and its duplication, kinetochores, and/or centromeres.

We irradiated our cells in G2 when duplication of the SPB is already completed, but the cells have not yet formed the mitotic spindle. As described above our preliminary results suggest that UVC-irradiated *rad3*Δ cells delay in G2 and not in mitosis. Therefore we think it unlikely that the SAC is responsible for the cell-cycle delay observed in *rad3*Δ cells.

An alternative candidate responsible for the mitotic delay of *rad3*Δ cells is Sty1. The Sty1 kinase is a MAP(mitogen-activated protein) kinase activated by various environmental stresses such as heat, oxidative stress and heavy metals but also by DNA damaging agents such as UVC or IR treatment. Rad3 and Sty1 share some of the same targets which include genes in the stress responses mentioned above (Alao & Sunnerhagen, 2008). Interestingly, Srk1 kinase, one of the proteins regulated by Sty1, is activated upon osmotic stress and causes phosphorylation

of Cdc25 at the same site as where Chk1 phosphorylates Cdc25, leading to cell cycle arrest (Lopez-Aviles *et al.*, 2005). Since Sty1 is activated by UVC light, it is tempting to think that a subsequent activation of the Sty1 target, Srk1, might be a mechanism that could keep *rad3*Δ cells arrested in G2 after UVC. In order to test the role of Srk1 and/or Sty1 in the cell cycle delay of *rad3*Δ cells, entry into mitosis could be monitored in *rad3*Δ*sty1*Δ and *rad3*Δ*srk1*Δ mutants.

Checkpoint arrest is important for cell survival after DNA damage because it allows time for the induction of repair mechanisms that eliminate the damage. *rad3*Δ cells have a low survival after UVC treatment in spite of arresting at G2/M, leading us to speculate that Rad3 might have a role in DNA repair.
It has been shown that Rad3 homologs in humans and budding yeast (ATR and Mec1, respectively) co-localize with replication protein A (RPA) at sites of DNA damage (Wu *et al.*, 2005; Nakada *et al.*, 2005). RPA is important in many DNA repair pathways including double strand brake repair by homologous recombination (HR). Following DNA damage RPA is phosphorylated by Phosphoinositide 3-kinase-related kinases including ATR and interacts with DNA repair proteins Rad51 and Rad52 (Binz *et al.*, 2004). Rad51 and Rad52 are important for homologous recombination which is the predominant repair pathway in G2. As DNA repair and checkpoint pathways are tightly coupled through RPA interacting both with Rad51/52 and ATR, a deletion of ATR might have an influence on DNA repair. Furthermore, ATR has been shown to phosphorylate XPA, an important component of the nucleotide excision repair (NER) pathway. Phosphorylation of XPA results in its increased nuclear localization and increased repair activity (Wu *et al.*, 2007; Shell *et al.*, 2009). Inefficient repair by HR and NER might well explain the profound UVC sensitivity of the *rad3*Δ mutant.

Appendix A.

Molecular weight standards

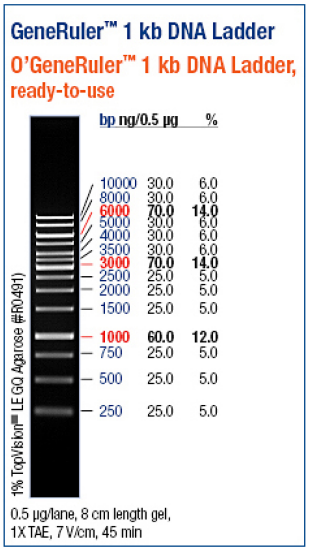

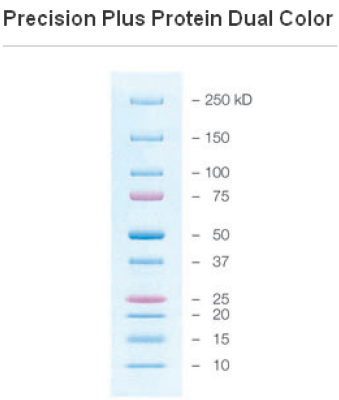

Bibliography

ALAO, J. P. & SUNNERHAGEN, P. (2008). Rad3 and Sty1 function in Schizosaccharomyces pombe: an integrated response to DNA damage and environmental stress? *Molecular Microbiology* **68**(2), 246–254.

ALBERTS, B., JOHNSON, A., LEWIS, J., RAFF, M., ROBERTS, K. & WALTER, P. (2008). *Molecular Biology of the Cell, 5th Edition*. Garland Science.

ALKHODAIRY, F. & CARR, A. M. (1992). DNA-repair mutants defining G2 checkpoint pathways in Schizosaccharomyces pombe. *Embo Journal* **11**(4), 1343–1350.

BENTLEY, N. J., HOLTZMAN, D. A., FLAGGS, G., KEEGAN, K. S., DEMAGGIO, A., FORD, J. C., HOEKSTRA, M. & CARR, A. M. (1996). The Schizosaccharomyces pombe rad3 checkpoint gene. *Embo Journal* **15**(23), 6641–6651.

BERG, J. M., TYMOCZKO, J. L. & STRYER, L. (2007). *Biochemie, 6.Auflage*. Elsevier GmbH, Spektrum Akademischer Verlag.

BINZ, S. K., SHEEHAN, A. M. & WOLD, M. S. (2004). Replication protein A phosphorylation and the cellular response to DNA damage. *DNA Repair (Amst.)* **3**, 1015–1024.

BROWN, T. A. (2006). *Genomes, Third Edition*. Garland Science.

CLERICI, M., BALDO, V., MANTIERO, D., LOTTERSBERGER, F., LUCCHINI, G. & LONGHESE, M. P. (2004). A tel1/mrx-dependent checkpoint inhibits the metaphase-to-anaphase transition after uv irradiation in the absence of mec1. *Mol Cell Biol* **24**(23), 10126–44.

DENG, J., HARDING, H. P., RAUGHT, B., GINGRAS, A. C., BERLANGA, J. J., SCHEUNER, D., KAUFMAN, R. J., RON, D. & SONENBERG, N. (2002). Activation of GCN2 in UV-irradiated cells inhibits translation. *Curr. Biol.* **12**, 1279–1286.

ELLEDGE, S. J., ZHOU, Z. & ALLEN, J. B. (1992). Ribonucleotide reductase: regulation, regulation, regulation. *Trends Biochem. Sci.* **17**, 119–123.

ENOCH, T., CARR, A. M. & NURSE, P. (1992). Fission yeast genes involved in coupling mitosis to completion of DNA replication. *Genes Dev.* **6**, 2035–2046.

ENOCH, T. & NURSE, P. (1990). Mutation of fission yeast cell cycle control genes abolishes dependence of mitosis on DNA replication. *Cell* **60**, 665–673.

FINGAR, D. C. & BLENIS, J. (2004). Target of rapamycin (TOR): an integrator of nutrient and growth factor signals and coordinator of cell growth and cell cycle progression. *Oncogene* **23**(18), 3151–3171.

FLETCHER, H., HICKEY, I. & WINTER, P. (2007). *Instant Notes Genetics, 3rd Edition*. Taylor & Francis Group.

FORSBURG, S. L. (2003a). Growth and manipulation of S. pombe. In: *Current Protocols in Molecular Biology*. John Wiley & Sons, Inc.

FORSBURG, S. L. (2003b). S. pombe strain maintenance and media. In: *Current Protocols in Molecular Biology*. John Wiley & Sons, Inc.

HAGAN, I. M. (1998). The fission yeast microtubule cytoskeleton. *J. Cell. Sci.* **111 (Pt 12)**, 1603–1612.

HINNEBUSCH, A. G. (2005). Translational regulation of GCN4 and the general amino acid control of yeast. *Annual Review of Microbiology* **59**, 407–450.

HUMPHREY, T. (2000). DNA damage and cell cycle control in Schizosaccharomyces pombe. *Mutation Research-Fundamental and Molecular Mechanisms of Mutagenesis* **451**(1-2), 211–226.

KASTAN, M. B. & BARTEK, J. (2004). Cell-cycle checkpoints and cancer. *Nature* **432**(7015), 316–23.

KILKENNY, M. L., DORE, A. S., ROE, S. M., NESTORAS, K., HO, J. C., WATTS, F. Z. & PEARL, L. H. (2008). Structural and functional analysis of the Crb2-BRCT2 domain reveals distinct roles in checkpoint signaling and DNA damage repair. *Genes Dev.* **22**, 2034–2047.

KNUTSEN, J. H., REIN, I. D., ROTHE, C., STOKKE, T., GRALLERT, B. & BOYE, E. (2011). Cell-cycle analysis of fission yeast cells by flow cytometry. *PLoS One* **6**(2), e17175.

KRAUSS, G. (2008). *Biochemistry of Signal Transduction and Regulation*. Weinheim: Wiley-VCH, 4th ed.

KROHN, M., SKJOLBERG, H. C., SOLTANI, H., GRALLERT, B. & BOYE, E. (2008). The G1-S checkpoint in fission yeast is not a general DNA damage checkpoint. *Journal of Cell Science* **121**(24), 4047–4054.

KUCSERA, J., YARITA, K. & TAKEO, K. (2000). Simple detection method for distinguishing dead and living yeast colonies. *Journal of Microbiological Methods* **41**(1), 19–21.

LEW, D. J. & BURKE, D. J. (2003). The spindle assembly and spindle position checkpoints. *Annu. Rev. Genet.* **37**, 251–282.

LOPEZ-AVILES, S., GRANDE, M., GONZALEZ, M., HELGESEN, A. L., ALEMANY, V., SANCHEZ-PIRIS, M., BACHS, O., MILLAR, J. B. & ALIGUE, R. (2005). Inactivation of the Cdc25 phosphatase by the stress-activated Srk1 kinase in fission yeast. *Mol. Cell* **17**, 49–59.

MORENO, S., KLAR, A. & NURSE, P. (1991). Molecular genetic-analysis of fission yeast Schizosaccharomyces-pombe. *Methods in Enzymology* **194**, 795–823.

MOSER, B. A. & RUSSEL, P. (2000). Cell cycle regulation in Schizosaccharomyces pombe. *Current Opinion in Microbiology* **3**, 631–636.

NAKADA, D., HIRANO, Y., TANAKA, Y. & SUGIMOTO, K. (2005). Role of the C terminus of Mec1 checkpoint kinase in its localization to sites of DNA damage. *Mol. Biol. Cell* **16**, 5227–5235.

O'CONNELL, M. J., WALWORTH, N. C. & CARR, A. M. (2000). The G2-phase DNA-damage checkpoint. *Trends in Cell Biology* **10**(7), 296–303.

PETERSEN, J. & NURSE, P. (2007). TOR signalling regulates mitotic commitment through the stress MAP kinase pathway and the Polo and Cdc2 kinases. *Nat Cell Biol* **9**(11), 1263–72.

POLLARD, T. D., EARNSHAW, W. C. & LIPPINCOTT-SCHWARTZ, J. (2007). *Cell Biology*. Heidelberg: Spektrum Akademischer Verlag, 2 ed.

SABATINOS, S. A. & FORSBURG, S. L. (2010). Molecular Genetics of Schizosaccharomyces pombe. In: *Methods in Enzymology* (JONATHAN, W., CHRISTINE, G. & GERALD, R. F., eds.), vol. Volume 470. Academic Press, pp. 759–795.

SHELL, S. M., LI, Z., SHKRIABAI, N., KVARATSKHELIA, M., BROSEY, C., SERRANO, M. A., CHAZIN, W. J., MUSICH, P. R. & ZOU, Y. (2009). Checkpoint kinase ATR promotes nucleotide excision repair of UV-induced DNA damage via physical interaction with xeroderma pigmentosum group A. *J. Biol. Chem.* **284**, 24213–24222.

TVEGARD, T., SOLTANI, H., SKJOLBERG, H. C., KROHN, M., NILSSEN, E. A., KEARSEY, S. E., GRALLERT, B. & BOYE, E. (2007). A novel checkpoint mechanism regulating the G1/S transition. *Genes & Development* **21**(6), 649–654.

WALKER, G. M. (1999). Synchronization of yeast cell populations. *Methods in Cell Science* **21**(2).

WATSON, J. D., BAKER, T. S., BELL, S. P., GANN, A., LEVINE, M. & LOSICK, R. (2008). *Molecular Biology of the Gene, 6. Edition*. Pearson International.

WEK, R. C. & STASCHKE, K. A. (2010). How do tumours adapt to nutrient stress? *EMBO J.* **29**, 1946–1947.

WOOD, V., GWILLIAM, R., RAJANDREAM, M. A., LYNE, M., LYNE, R., STEWART, A., SGOUROS, J., PEAT, N., HAYLES, J., BAKER, S., BASHAM, D., BOWMAN, S., BROOKS, K., BROWN, D., BROWN, S., CHILLINGWORTH, T., CHURCHER, C., COLLINS, M., CONNOR, R., CRONIN, A., DAVIS, P., FELTWELL, T., FRASER, A., GENTLES, S., GOBLE, A., HAMLIN, N., HARRIS, D., HIDALGO, J., HODGSON, G., HOLROYD, S., HORNSBY, T., HOWARTH, S., HUCKLE, E. J., HUNT, S., JAGELS, K., JAMES, K., JONES, L., JONES, M., LEATHER, S., MCDONALD, S., MCLEAN, J., MOONEY, P., MOULE, S., MUNGALL, K., MURPHY, L., NIBLETT, D., ODELL, C., OLIVER, K., O'NEIL, S., PEARSON, D., QUAIL, M. A., RABBINOWITSCH, E., RUTHERFORD, K., RUTTER, S., SAUNDERS, D., SEEGER, K., SHARP, S., SKELTON, J., SIMMONDS, M., SQUARES, R., SQUARES, S., STEVENS, K., TAYLOR, K., TAYLOR, R. G., TIVEY, A., WALSH, S., WARREN, T., WHITEHEAD, S., WOODWARD, J., VOLCKAERT, G., AERT, R., ROBBEN, J., GRYMONPREZ, B., WELTJENS, I., VANSTREELS, E., RIEGER, M., SCHAFER, M., MULLER-AUER, S., GABEL, C., FUCHS, M., FRITZC, C., HOLZER, E., MOESTL, D., HILBERT, H., BORZYM, K., LANGER, I., BECK, A., LEHRACH, H., REINHARDT, R., POHL, T. M., EGER, P., ZIMMERMANN, W., WEDLER, H., WAMBUTT, R., PURNELLE, B., GOFFEAU, A., CADIEU, E., DREANO, S., GLOUX, S., LELAURE, V. *et al.* (2002). The genome sequence of Schizosaccharomyces pombe. *Nature* **415**(6874), 871–880.

WU, X., SHELL, S. M., LIU, Y. & ZOU, Y. (2007). ATR-dependent checkpoint modulates XPA nuclear import in response to UV irradiation. *Oncogene* **26**, 757–764.

WU, X., YANG, Z., LIU, Y. & ZOU, Y. (2005). Preferential localization of hyperphosphorylated replication protein A to double-strand break repair and checkpoint complexes upon DNA damage. *Biochem. J.* **391**, 473–480.

YE, J. B., KUMANOVA, M., HART, L. S., SLOANE, K., ZHANG, H. Y., DE PANIS, D. N., BOBROVNIKOVA-MARJON, E., DIEHL, J. A., RON, D. & KOUMENIS, C. (2010). The GCN2-ATF4 pathway is critical for tumour cell survival and proliferation in response to nutrient deprivation. *Embo Journal* **29**(12), 2082–2096.

Acknowledgments

This master thesis was carried out in the Department of Cell Biology, Institute for Cancer Research, The Norwegian Radium Hospital. This thesis would not have been accomplished without the support from a number of people which I would like to thank.

I would like to thank Professor Erik Boye for his ongoing support and encouragement in this research project as well as critical reading of my thesis.

I would like to express my sincere gratitude to my supervisor Dr. Beata Grallert for introducing me to the field of cell-cycle regulation in *S.pombe* and for sharing her great knowledge with me. Thank you for your guidance and support both in the lab and in the process of writing this thesis.

Thanks to the whole pombe group for all the help and support I got during my work. I am grateful to Jon Halvor Knutsen for teaching me how to use the flow cytometer and how to analyze the results. Thank you for your patience and time to discuss all my small questions. Special thanks to Gro Elise Røland for helping me with the lactose gradients and the good company in the lab. Thanks also for reading my thesis.

Thanks to Riikka and Mahsa. It is so much fun to share the office with you. I especially appreciate our coffee breaks with Iranian cookies or Finnish apple cake!

A special thanks to Gry and Jonny, Astrid and Lars Egil. Thanks for your support during my whole time here in Norway and for the many dinners introducing me to "strange" Norwegian food.

Mein besonderer Dank gilt meiner Familie, die immer für mich da ist und mich mein ganzes Studium unterstützt hat. Danke an Matze, meinen Lieblingsbruder, für die Unterstützung beim Erlernen von LATEX und für das Lösen der vielen kleinen Probleme die während des Schreibens auftauchten. Danke für Deine Geduld und das Interesse an meiner Arbeit.

Christiane Rothe Oslo, June 2011